11-2022

Pile-Supported Wharves Subjected to Inertial Loads and Lateral Ground Deformations. II: Guidelines for Equivalent Static Analysis

Milad Souri
Portland State University, msouri@pdx.edu

Arash Khosravifar
Portland State University, karash@pdx.edu

Stephen E. Dickenson
New Albion Geotechnical

Scott Schlechter
GRI

Nason McCullough
Jacobs Engineering Group

Citation Details

Published as: Souri, M., Khosravifar, A., Dickenson, S., Schlechter, S., & McCullough, N. (2022). Pile-supported wharves subjected to inertial loads and lateral ground deformations. II: Guidelines for equivalent static analysis. Journal of Geotechnical and Geoenvironmental Engineering, 148(11), 04022091.

Pile-supported wharves subjected to inertial loads and lateral ground deformations. II: Guidelines for equivalent static analysis

Milad Souri[1], Arash Khosravifar, Ph.D., P.E. M.ASCE[2], Stephen Dickenson, Ph.D., P.E., D. PE, M. ASCE[3], Scott Schlechter, P.E., G.E., M.ASCE[4], Nason McCullough, Ph.D., P.E., G.E., M.ASCE[5]

[1] Graduate Student, Portland State University, Portland, OR 97201; e-mail: msouri@pdx.edu

[2] Corresponding author, Assistant Professor, Portland State University, Portland, OR 97201; e-mail: karash@pdx.edu

[3] Principal Engineer, New Albion Geotechnical, Inc., Reno, NV 89509; e-mail: sed@newalbiongeotechnical.com

[4] Principal, GRI, Beaverton, OR 97008; e-mail: SSchlechter@gri.com

[5] Principal Geotechnical Engineer, Jacobs, Corvallis, OR 97330; e-mail: Nason.McCullough@jacobs.com

ABSTRACT

An equivalent static analysis (ESA) procedure is proposed for the design of pile-supported wharves subjected to combined inertial and kinematic loads during earthquakes. The accuracy of the ESA procedure is evaluated against measurements from five large-scale centrifuge tests. The wharf structures in these tests were subjected to a suite of recorded ground motions and the associated superstructure inertia as well as earthquake-induced slope deformations of varying magnitudes. It is shown that large bending moments at depths greater than 10 pile diameters are primarily induced by kinematic demands and can be estimated by applying soil displacements only (i.e., 100% kinematic). In contrast, the large bending moments at the pile head are primarily induced by wharf deck inertia and can be estimated by applying superstructure inertial loads at the pile head only (i.e., 100% inertial). The large bending moments at depths shallower than 10 pile diameters are affected by both inertial and kinematic loads; therefore, the evaluation of pile performance should include soil displacements and a portion of the peak inertial load at the pile head that coincides with the peak kinematic loads. Ranges for inertial and kinematic load combinations in uncoupled analyses are provided for different soil profiles. The details on the back-calculated load combination factors are provided in the companion paper.

INTRODUCTION

Pile-supported wharves must be designed to accommodate superstructure inertial loads imposed at the pile head and kinematic loads imposed on the piles from the lateral ground deformations when subjected to earthquake motions. Lateral ground deformations may be caused by inertial slope movement, and/or by lateral spreading from liquefaction or cyclic softening of foundation soils in sloping ground adjacent to the structure and in the backland areas. However, there is no consensus in existing guidelines for pile design on how to combine inertial loads and kinematic demands from lateral ground deformations.

The damage to pile-supported bridges and wharves due to liquefaction-induced lateral spreading has been documented in a number of case histories, e.g., 1964 Niigata earthquake (Hamada et al. 1986), 1989 Loma Prieta earthquake (Donahue et al. 2005), 1995 Kobe earthquake (Tokimatsu and Asaka 1998), 2010 Haiti earthquake (Rathje et al. 2010), 2010 El Mayor-Cucapah earthquake (Turner et al. 2016), and 2016 Kaikoura earthquake (Cubrinovski et al. 2017). In most of these studies, the lateral spreading displacements exceeding 1 m were reported as the likely cause of damage. While some studies back-calculated the likely combination of superstructure inertia and lateral spreading demands (e.g., Turner et al. 2016), the exact interaction of inertia and lateral spreading loads could not be directly calculated in these case histories due to the lack of strong motion instrumentation on the superstructure and the soil, and lack of data necessary to establish the pattern of soil deformations with depth. The paucity of well-instrumented sites at ports subjected to damaging earthquakes has necessitated the use of numerical and physical models to evaluate the phasing and relative impact of inertial and kinematic loads in piles. The robust data set from five centrifuge tests on pile-supported wharves performed by McCullough et al. (2007) has been thoroughly re-evaluated and used in this study to address previously unexamined aspects of dynamic soil-pile interaction. These models included instrumented superstructure deck and piles and embedded sensors within the soil profile. These tests provided a unique opportunity to back-calculate the inertial and kinematic loads combination factors for equivalent static analysis.

Different design guidelines provide varying recommendations on how to combine superstructure inertial and kinematic ground deformation loads to estimate the lateral demands on piles. MCEER/ATC (2003) states that for most earthquakes the peak inertia is likely to occur early in the ground motion while the maximum lateral spreading load will develop near the end of motion. Consequently, it recommended designing piles for independent effects of inertia and lateral spreading.

Boulanger and coworkers performed a series of 14 centrifuge tests on piles in liquefiable soils (Boulanger et al. 1999; Brandenberg et al. 2007). They recommended combining the full residual lateral spreading load with 65% to 85% of the peak inertial load, in contrast to the recommendations put forth in MCEER/ATC (Boulanger et al. 2007; Ashford et al. 2011).

Researchers at Rensselaer Polytechnic Institute (RPI) have performed many centrifuge tests on piles in liquefiable soils. Abdoun and Dobry (2002) showed that while the bending moments at depths shallower than 2 or 3 m are affected by superstructure inertia, this effect disappeared for bending moments at deeper depths for 0.6-m-diameter piles. They also reported a post-peak reduction in the lateral spreading force despite the increase in ground displacement (Dobry et al. 2003; Abdoun et al. 2003). Olson et al. (2017) performed another series of four centrifuge tests at RPI to investigate the magnitude of lateral spreading force on large-diameter foundations. The latter tests focused on the kinematic effects, and the effects of inertia were not considered.

Tokimatsu et al. (2005) performed large-scale 1-g shake table tests in Japan's NIED facility to study phasing of inertia and liquefaction-induced lateral spreading. They concluded that the inertial and lateral spreading loads were in-phase for structures having a natural period shorter than the natural period of the ground ($T_{structure}<T_{ground}$), and the two loads were out-of-phase for $T_{structure}>T_{ground}$.

Cubrinovski et al. (2014) developed a design guideline for liquefaction and lateral spreading effects on highway bridges in New Zealand. They separated the development of kinematic loading due to soil displacements into a cyclic phase and a spreading phase. While they recommended a combination of the inertial load with kinematic loads for the transient, cyclic phase, they stated that the combination of the two loads may or may not be considered for the spreading phase at the discretion of the engineer.

The design guidelines provided in commonly used codes for wharves and piers are summarized in Table 1. ASCE 61-14 (ASCE 2014) requires that simultaneous application of inertial and kinematic loads be considered, taking into account the phasing and the locations where the loads are applied. The commentary in Section C4.7 of ASCE 61-14 and the Port of Long Beach Wharf Design Criteria (POLB 2015) suggest that the locations of maximum bending moments from inertia and lateral ground deformations are spaced far enough apart that the two loads do not need to be superimposed. They also suggest that the maximum bending moments from the two loads tend to occur at different times; therefore, they recommend that the loads be treated as uncoupled for typical marginal container wharves. On the other hand, Port of Anchorage Modernization Program Seismic Design Manual (POA 2017) recommends combining the peak inertial loading from earthquake ground motions with 100% of peak kinematic loads from lateral ground displacements. This design manual allows for smaller combination factors (no less than 25%) if justified using peer-reviewed 2-D nonlinear numerical analysis.

The design recommendations for pile-supported highway bridges also vary significantly as summarized in Table 1. The transportation agencies in California and Oregon require combining 100% lateral spreading with 50% inertia (Caltrans 2012; ODOT 2014); Caltrans later retracted this recommendation in favor of higher performance criteria (Caltrans 2016). Washington State DOT recommends 100% lateral spreading + 25% inertia (WSDOT 2021), while AASHTO (2014) recommends designing piles for the simultaneous effects of inertia and lateral spreading only for large magnitude earthquakes (M>8).

The varying recommendations provided by highway and maritime transportation agencies highlight the site- and project-specific assumptions that are made to combine inertial and kinematic demands on piles. It is recognized that there is limited research and validation of these assumptions, and most design codes indicate that these assumptions should be evaluated on a project-specific basis.

This paper summarizes the development of a practice-oriented equivalent static analysis (ESA) procedure using p-y models for the design of pile-supported wharves subjected to lateral ground deformations during earthquake loading. The accuracy of the ESA procedures in estimating pile demands is evaluated against the results of five centrifuge tests on pile-supported wharves. The piles in these centrifuge tests were subjected to the combined effects of wharf deck inertial loads and ground deformations. The experiments included soil properties ranging from nonliquefiable to fully liquefied cases, providing a wide range of conditions against which the ESA method could be evaluated. Additionally, these tests included the system-level response of the wharf deck and all rigidly-connected piles, as opposed to single piles, as had been used in most of the centrifuge-based investigations previously cited. This is important because the restraining effects of the superstructure affect how inertial and kinematic loads interact, as reported by Turner et al. (2016). The following section of this paper provides an overview of the five centrifuge tests that were used in this study. The paper is then followed by two sections where peak inertial and peak kinematic demands are estimated and compared with centrifuge measurements. Next, load factors to combine peak inertial and peak kinematic loads are presented. Concluding remarks are provided based on a comparison of the demands estimated from ESA to those measured in the centrifuge tests. A design example is provided to summarize the implementation of the recommended procedure in design.

CENTRIFUGE TESTS

Details for the centrifuge tests can be found in a series of data reports in McCullough et al. (2000), Schlechter et al. (2000a, b), and Boland et al. (2001a, b). The pile, superstructure, and soil properties and the applied input motions are provided in the companion paper (Souri et al. 2022). The methods of re-evaluation and re-interpretation of the carefully curated data set are also addressed in the companion paper. All tests included a wharf deck supported by 21 piles configured in a 7-by-3 setup. The piles consisted of aluminum pipe piles with outer diameters ranging from 0.38 m to 0.64 m (in prototype scale). The centrifuge scale factor was 40.1 for all tests.

Fig. 1 shows the cross sections of the five centrifuge models. The subsurface conditions in model NJM01 included a multi-lift rock dike, a loose sand layer that liquefied during shaking and resulted in lateral spreading, a dense sand layer above the water table, and a dense sand layer at the pile tips. A relatively soft Bay Mud layer was included in model NJM02, while a cement-deep-soil-mixing (CDSM) unit was incorporated into model SMS01. Model SMS02 featured a single, monolithic rock dike supported by a dense layer of sand. In model JCB01, the rock dikes were replaced with a thin layer of rock simulating an armour, wave protection layer. The failure surfaces in each model, indicated in Fig. 1 with red dashed lines, were determined based on the soil displacement profiles interpreted from accelerometer data. In general, the observed zone of shear failure in the liquefied sand in the vicinity of piles can be characterized as broad, diffuse shear failure combined with a localized shear plane at the interface of weak and resistant layers (such as liquefied sand and upper rockfill). Localized shear planes were also developed above the Bay Mud layer in NJM02 and below the CDSM unit in SMS01, which contributed to the large pile bending moments that developed at depth in these two models. The overall objective of the current study was to develop guidelines for combining inertial and kinematic demands in ESA and to evaluate their accuracy in estimating the large bending moments that were observed in the centrifuge tests.

ESTIMATING PEAK KINEMATIC DEMANDS

The estimation of kinematic demands on piles is routinely made in practice using slope deformations computed using simplified Newmark sliding block analysis (Newmark 1965) and application of the approximated free-field soil deformation pattern to p-y springs connected to the piles. The use of more complex and detailed two- or three-dimensional dynamic analysis that incorporates coupled soil–structure interaction is also common, and often compared with the results of the practical initial analysis. In the subsequent analysis completed in this investigation, the soil displacements were computed using the Newmark method and were applied to the end nodes of p-y springs using beam on nonlinear Winkler foundation (BNWF) approach. One pertinent question in this method of analysis is whether the permanent, residual soil displacement (at the end of shaking) or the peak transient soil displacement (which occurs during shaking) should be used in design to evaluate the kinematic pile demands. ASCE 61-14 (Section 4.7.2) specifically requires that the permanent portion of the lateral ground deformations be used to estimate the kinematic demands on piles. However, it has been shown in Souri et al. (2019) that the peak transient bending moments at both the pile head and at depth are often greater than the residual bending moments at the end of shaking; this result was attributed, partly, to the difference between the peak transient soil displacement and the permanent soil displacement. The following section provides practical guidelines for design by comparing the estimated soil displacements against the measurements obtained from the centrifuge tests.

Estimating Soil Displacements at the Ground Surface

Estimation of Soil Displacements using the Newmark Sliding Block Method

Permanent ground displacements were estimated using the Newmark sliding block method (hereafter referred to as *Newmark analysis*). The yield accelerations for each test were determined by using pseudo-static limit equilibrium analysis and were assumed to be constant during the motion in the Newmark analysis. The beneficial resistance of the piles against the laterally moving ground (i.e., the pile pinning effects) were considered by including the piles as reinforcement elements in the limit equilibrium analysis. Thus, the soil displacements calculated here are pile-restrained displacements and not free-field displacements. The residual strength for liquefied soils in the limit equilibrium analysis was determined using correlations and were consistent with the weighted approach proposed by Kramer (2008). If liquefaction was not triggered, an equivalent friction angle was calculated proportional to the pore water pressure ratio using the relationship by Ebeling and Morrison (1992). Full details for these analyses are provided in McCullough et al. (2001). The yield accelerations used in the Newmark sliding block analysis are reported in Supplemental Appendix B. Newmark analyses are typically performed in practical applications using accelerations that are obtained from site response modeling; however, in this study, the recorded accelerations from centrifuge tests were used as input for the Newmark analysis. Thus, uncertainties in ground motion estimation associated with site response analysis are minimized.

Comparison between the Soil Displacements from Centrifuge Tests and Newmark Analysis

The accuracy of the Newmark method in estimating soil displacements was evaluated by comparing the results of the Newmark analysis to the measured displacements obtained from the centrifuge tests. Fig. 2 shows a comparison of median Newmark displacements for all accelerometers within the failure mass against the permanent displacement (end of shaking) and peak transient displacement measured at the ground surface in the centrifuge tests. The vertical bars show the Newmark median + 1σ and Newmark median − 1σ values. The Newmark displacements include the pile-pinning effects. The centrifuge displacements were calculated by combining high-frequency and low-frequency components of displacements using data from the linear variable differential transformer (LVDT) and accelerometers that were installed in the vicinity of the piles; therefore, the displacements shown in Fig. 2 can be considered pile-restrained. All displacements are adjusted to be relative to the base of the model. This figure suggests that the permanent (end of shaking) displacements from the centrifuge tests are better estimated using the median Newmark displacements; however, this analytical approach tended to overestimate the observed displacements by roughly 10%, on average. This figure also suggests that the peak transient displacements from the centrifuge tests are better estimated using the median + 1σ displacements from the Newmark analysis, and in this case the simplified sliding block model tends to underestimate the peak displacement by roughly 10%. For comparison, the peak transient displacements from the centrifuge tests are underestimated by median Newmark displacements by approximately 50%. The measured peak transient displacements were found to be between 1.2 and 7.5 times larger than the permanent displacements in most cases (with the larger ratios corresponding to nonliquefied soil profiles). The median + 1σ displacements from Newmark were, on average, 1.8 times larger than the median Newmark displacements.

The difference between the permanent displacement and peak transient displacement should be considered in conjunction with the distribution of soil displacements with depth in the pseudo-static analysis. While Fig. 2 illustrates that the median Newmark displacements underestimated the peak transient soil displacements, it will be shown that the distinct transitions in the idealized soil displacement profiles resulted in overestimation of the predicted pile bending moments such that the combination of median Newmark displacements and an idealized soil displacement profile resulted in satisfactory estimates of the peak pile bending moments.

Estimating Soil Displacements with Depth

Idealized Soil Displacement Profile with Depth

Cubrinovski et al. (2014) showed that the lateral displacement index (LDI) approach (Zhang et al. 2004; Idriss and Boulanger 2008) can be used to estimate the shape of soil displacement profile with depth. They found that the ground surface displacements computed from the LDI approach were two to three times larger than the measured free-field displacements in the case histories pertaining to damaged bridges during the 2010-2011 Canterbury, New Zealand earthquakes. Therefore, they used the measured displacements at the ground surface and distributed it with depth based on the shape of the displacement profile from the LDI approach. The LDI approach includes integrating the maximum shear strains in all soil layers to develop the soil displacement profile. Armstrong et al. (2014) used a similar approach where they used the LDI approach to estimate the displacement profile with depth and then scaled it down to match the ground surface displacement estimated from the Newmark method. Using the LDI approach for the five sets of centrifuge models resulted in approximately linear deformations with depth within the loose sand layer and negligible deformations in the rockfill and dense sand layers. Therefore, the idealized soil displacement profiles in this study were simply assumed to vary linearly with depth within the loose sand units and remain constant within the rockfill and the dense sands units. The idealized soil displacements profiles are referred to as "design" soil displacements hereafter.

Soil Displacement Profiles Obtained from Centrifuge Tests

To evaluate the accuracy of the design soil displacement profiles, it was necessary to develop the soil displacement profiles in each of the centrifuge tests. The horizontal soil displacements at a given depth below the ground surface were calculated by combining the high-frequency and low-frequency components of the displacements. Following the procedure explained by Wilson (1998), the high-frequency component of soil displacements was calculated by double integration of the recorded accelerations from the embedded accelerometers and were filtered by applying a high-pass Butterworth filter with a corner frequency of 0.25 Hz. The low-frequency component of soil displacements at a given depth were calculated by applying a low-pass Butterworth filter with the same corner frequency to the recorded LVDT displacement at the ground surface and then distributing it with depth based on an assumed profile. This profile was developed using the shape of the maximum transient displacements with depth obtained from the accelerometer data as a guide. No permanent soil displacement was considered below the shear failure plane. The pattern of the permanent accumulated soil displacements with depth generally agreed with the measurements on the dissected model, which were made after the tests were completed. The baseline analysis that is described later in the paper provides a measure of accuracy of the interpreted soil displacements from centrifuge tests by comparing the computed and measured bending moments in piles.

Comparison Between Centrifuge and Design Soil Displacement Profiles

A comparison of soil displacement profiles from centrifuge tests and design is shown in Fig. 3 for Event 11 of model NJM01. The soil displacements were interpreted at the pile locations to be applied to the end nodes of p-y springs. The design soil displacements were estimated using the mean Newmark displacements, and the centrifuge soil displacements correspond to the peak transient displacement during motion (which occurred at time t = 21.6 sec). It can be observed from this figure that for piles in rows 1, 2 and 3, where the kinematic effects are large, the peak transient soil displacements are underestimated by the mean Newmark displacements by approximately 33% (i.e. the ratio of estimated displacements at the top of the slope from Newmark to interpreted displacements from centrifuge was 0.67). While the design soil displacement profile follows the general trends observed in the centrifuge tests, it lacks the smooth curvature of the displacements at the boundary of rockfill and loose sand and the localized curvature within the loose sand from the centrifuge test.

The same trend for soil displacements interpreted from centrifuge tests and estimated in design for model NJM01 was consistently observed in other centrifuge tests. In the results for all five tests shown in Fig. 4, the peak transient soil displacements from the centrifuge tests were generally underestimated when evaluated using the mean Newmark values (the ratio of estimated displacements at top of the slope from Newmark to interpreted displacements from centrifuge ranged from 0.13 to 1.21). This is important considering that mean Newmark displacements are typically recommended by design guidelines to evaluate the permanent (not peak transient) lateral ground deformations and the associated kinematic demands (e.g., ASCE 61-14). However, we found that the distinct transitions in the idealized soil displacement profiles at layer boundaries above and below the loose sand layer over-predict the pile bending moments. These two effects have an approximately equal and opposite influence on the estimated bending moments, such that the combination of idealized soil displacement profiles and mean Newmark displacements provided reasonable estimations of computed peak transient pile bending moments. This is shown in Fig. 5 for Pile 1 in NJM01-Event 11 as an example. Fig. 5a shows two different soil displacement profiles: (a) interpreted from centrifuge exhibiting a ground surface displacement of 0.13 m and smooth transitions at layer boundaries, and (b) estimated from Newmark exhibiting a ground surface displacement of 0.09 m and an idealized "design" distribution of displacements with depth with distinct transitions at layer boundaries. Fig. 5b shows the bending moments along the pile calculated by exerting the two soil displacement profiles to the end nodes of p-y springs in a pseudo static analysis (details for the developed p-y models are provided later in this paper). This figure shows that the maximum deep bending moment at the boundary between liquefied sand and the lower dense sand is fairly similar between the two approaches (1116 kN-m in the case of using centrifuge displacements and 1101 kN-m in the case of using design soil displacements). For comparison, the measured peak bending moments from centrifuge are also plotted in this figure. The reasonable agreement between the measured bending moments and the estimated bending moments by applying interpreted soil displacements from centrifuge confirms that the assumptions made in interpreting soil displacement profiles with depth by combining the high- and low-frequency components of embedded accelerometer data and LVDT at the ground surface were reasonable. The discrepancy between the curvature of the estimated and interpreted soil displacement profiles at layer boundaries was also reported in other studies involving centrifuge tests and numerical analyses (e.g., Brandenberg et al. 2007; McGann et al. 2011; Armstrong et al. 2014). Caltrans (2012) recommends tapering the p-y spring properties over a transitional zone that extends one to two pile diameters from the interface between the liquefied and nonliquefied layers; this approach was adopted in this study.

Lateral Soil Reactions on Piles at the Time of Maximum Bending Moment

The lateral soil reactions back-calculated from the centrifuge tests showed that the nonliquefied rockfill does not apply a uniformly bayward (i.e., downslope) pressure. Rather, the direction of the transient lateral soil reaction changes throughout the rockfill. The cross sections of two tests where the pile instrumentation was dense enough to accurately compute the soil reactions are shown in Fig. 6. The soil reactions were computed by fitting a spline curve to the bending moments and a double differentiation with depth (Souri et al. 2020). The profiles show the lateral soil reactions that occur at the time of maximum bending moments. The soil reactions plotted in this figure are all based on experimental results. In Piles 1 and 2 of NJM01 and in Piles 2 and 5 of SMS01, where a thick nonliquefiable crust (rockfill) was present, the top portion of the crust was resisting the inertial load, as indicated by positive (landward) soil reactions. The inertial force at the pile head was bayward. In these models, the effect of inertia was resisted by the resisting lateral soil pressure from the nonliquefied crust, and it did not contribute to the bending moments that developed at depth (~20 m below the pile head in NJM01 and ~22 m below the pile head in SMS01). It is important to note that in both tests the rockfill moved almost uniformly over the liquefied soils. This observation is further analyzed in Fig. 7 for Pile 1 in NJM01 Event 11, as an example. The soil and pile displacement profiles are plotted at the time of maximum bending moment (Fig. 7a) showing that the pile has moved more than the soil in the top half portion of the rockfill resulting in a positive (landward) soil reaction (Figs. 7b and 7c). Conversely, the soil has moved more than the pile in the bottom half portion of the rockfill resulting in a negative (bayward) soil reaction. The inertial force at the pile head was bayward as indicated by the slope of the bending moments at the pile head (Fig. 7d). Figure 7b and 7c show the same data but at different scales. The ultimate soil reactions (p_u) were calculated based on commonly used p-y relationships for sand proposed by American Petroleum Institute (API 1993) and are plotted in this figure as a reference (details and input parameters for API model are provided in Supplemental Appendix A). This comparison shows that the soil reactions are significantly smaller than the full passive pressure. This is expected for relatively flexible piles used in this study as the piles closely follow the soil deformations. This conclusion is likely to be different for relatively stiff piles such as large diameter shafts as the soil deformations could be much larger than the pile deformations to the extent that full passive pressure may develop throughout the nonliquefied crust. This finding is consistent with those in Boulanger et al. (2007), which showed that with relatively flexible piles, the nonliquefiable crust load can, in fact, apply a resisting upslope reaction while the inertia is downslope.

The observations made regarding models NJM01 and SMS01 suggest that it is overly conservative to estimate the kinematic demands by applying a bayward limiting pressure throughout the entire rockfill. Thus, for the piles analyzed in this study, it was more appropriate to apply kinematic demands by imposing the estimated soil displacements (including pile-pinning effects) to the end nodes of the p-y springs.

DEVELOPING P-Y MODELS FOR EQUIVALENT STATIC ANALYSIS

Nonlinear beam on Winkler foundation models (i.e. p-y models) were developed for equivalent static analysis. The p-y models were created in *LPILE* v. 2019 (Ensoft 2016) and were calibrated using four static lateral load pile tests that were performed for SMS02 and JCB01. A summary of these calibrations is provided in the Supplemental Appendix A. More details on calibrations of *LPILE* models are provided in Souri et al. (2020). A baseline analysis was performed to measure the accuracy of assumptions in developing p-y spring properties, p-multipliers, and soil displacement profiles.

Soil Properties

The moduli of the subgrade reaction for sand were modified from the API recommendations to match the results of the four static lateral load tests. The rockfill was modeled by incorporating a pseudo-cohesion of 15 kPa to account for additional resistance caused by the interlocking and movement of rock particles near the ground surface, and stress-dependent strength at very low confining stress thus simply modeled as a ϕ'-c' soil as applied in calibration studies from field load tests in rockfill (e.g. McCullough and Dickenson 2004; Dickenson et al. 2016). No modifications were made to the p-y springs in regard to the ground slope as the p-y models reasonably captured the pushover curves and pile demands from the four static lateral load tests as described in Souri et al. (2020).

Pile Properties

The wharf deck in the centrifuge tests was supported by three rows of seven piles (for a total of 21 piles) with diameters ranging from 0.38 m to 0.64 m. Considering the rigidity of the wharf deck, all piles were assumed to have zero rotation at the pile head. The piles remained elastic in the centrifuge tests and were modeled as elastic in the *LPILE* models. While the piles in the centrifuge tests were hollow aluminum pipes, their stiffness properties in prototype scale represented those of prestressed concrete piles.

P-multipliers

The p-y springs were modified using p-multipliers (P_m) proportional to the pore water pressure ratio R_u generated during the ground motion: $P_m = 1.2 - 1.1*Ru$ for $Ru > 0.2$ and $P_m = 1.0$ for $Ru \leq 0.2$, as the effect of liquefaction is assumed to be negligible when Ru is below 0.2. These practice-oriented relationships account for the first-order softening effect of liquefaction and generally agree with the nonlinear relationship proposed by Liu and Dobry (1995). For details on the development of the proposed R_u-proportional p-multipliers for liquefiable soils and their effectiveness in predicting peak pile demands, see Souri et al. (2020). In this study, the Ru values recorded in the vicinity of piles were used. In practice, these values can be estimated from simplified correlations with the factor of safety against liquefaction.

Baseline Analysis – Accuracy of Modeling Assumptions

There are several sources of uncertainty in performing equivalent static analysis including (a) numerical modeling approach (e.g., p-y spring properties, pile properties, and boundary conditions), (b) estimating kinematic demands from soil displacements, (c) estimating inertial demands associated with superstructure mass, and (d) combining inertial and kinematic demands in equivalent static analysis. The baseline analysis described in this section provides a measure of accuracy of the assumptions that were made during the numerical modeling approach (item a) and in estimating the soil displacement profiles (item b). The accuracy of assumptions made in estimating inertial demands and the combination of inertial and kinematic demands are assessed later in this paper.

The baseline analyses consist of applying the interpreted soil displacements from centrifuge ("centrifuge" displacements shown in Fig. 4) to the end nodes of p-y springs in the calibrated *LPILE* models. The inertial loads at top of the piles were directly calculated from centrifuge tests by differentiating the bending moments at top of the piles for cases where at least two strain gauges were installed between the top of the pile and the ground surface. It is worth noting that equivalent static analysis inherently suffers from simplifying a dynamic response including soil-pile-structure interaction and liquefaction-induced softening of soils to a static analysis. The accuracy of these assumptions and simplifications are assessed in this section by comparing the measured and computed bending moments.

Fig. 8 shows the computed and measured bending moments for NJM01-Event 11 as an example. The measured bending moments correspond to the peak values during motion measured at time t = 21.6 sec. While the time of maximum bending moment was found to generally vary with pile row and depth, in NJM01-Event 11 specifically, the maximum bending moment in all instrumented piles occurred at approximately the same time (i.e. t = 21.6 sec). The locations of large bending moments are color-coded: bending moments above grade are shown in red, and those below grade are shown in blue, noting that deep bending moments below grade are specifically affected by the shape and magnitude of exerted soil displacement profiles. Close agreement is observed between the measured and estimated bending moments, which justifies the assumptions that were made in developing the p-y models and the interpreted soil displacement profiles from centrifuge. The maximum bending moments along the piles are compared for all five tests and two shaking events for each test in Fig. 9. This figure shows the accuracy in measuring the bending moments in piles subjected to liquefaction and lateral spreading loads using the calibrated *LPILE* models in equivalent static analysis. The bending moments below grade are plotted in blue and those above grade (i.e. at pile head) are plotted in red. On average, the estimated bending moments using *LPILE* are 5% larger than the measured bending moments while the majority of the data points are bounded within the 1:2 and 2:1 lines (with the exception of two data points with very small bending moments).

ESTIMATING PEAK INERTIAL DEMANDS

Equivalent non-linear static analysis (ESA) was used to estimate the peak inertial demands associated with the dynamic response of the deck mass. The ESA procedure included developing p-y models for a single row of piles, developing a lateral force-displacement relationship (pushover curve) for the entire pile group, calculating the equivalent stiffness and natural period of the wharf, and estimating the peak inertial force using the acceleration response spectra at the ground surface. The ESA was performed for both liquefied and nonliquefied conditions. The estimated inertial demands were then compared against the measured demands from the centrifuge tests to evaluate the accuracy of the ESA procedures. It is worth noting that there are other important variables in performing ESA that were not evaluated in this study, such as the uncertainties associated with the p-y spring properties in the design as recommended by ASCE 61-14 (ASCE 2014), the effect of pile head fixity on the lateral stiffness of the pile group, and the uncertainties associated with site response analysis. These are complex, project-specific issues, which warrants additional investigation of the sensitivity of the load combinations to these uncertainties.

Pile Group Force–Displacement Relationships

Force–displacement relationships (i.e., pushover curves) were developed for the entire pile group for each centrifuge test under the two conditions shown in Fig. 10. In the nonliquefied condition (Case A), regular p-y springs were used with no soil displacements. For the liquefied condition (Case B), soil displacements were imposed to the end nodes of the p-y springs, and the p-y curves for the liquefiable soils were softened using p-multipliers. The mean Newmark soil displacements were distributed with depth using an idealized profile, as this combination reasonably predicted the peak bending moments in the centrifuge tests. The idealized soil displacements used in Case A analyses are the ones labeled as "Design" in Fig. 4. To develop pushover curves using *LPILE* models, displacements were imposed incrementally at the top of individual piles while maintaining zero rotation at the pile head to simulate the rigid connection between the piles and the wharf deck. The total shear force for the pile group was calculated by summing the pile head shear forces of all seven piles in one row multiplied by three rows in the transverse direction. No group reduction factor was considered based on AASHTO (2014), since the pile spacing was greater than six times the pile diameter. Some studies have shown that the sequence of applying inertial and kinematic demands can affect the estimated demands on piles (e.g. Chang 2007). However, this topic was not investigated in this study; thus, the full soil displacement was applied in *LPILE,* and the pile head displacements were incrementally increased to reach 1 m.

The pushover curves are shown in Fig. 11 for all five sets of centrifuge test models. The pushover curves for the liquefied condition are different for each shaking because the soil displacements are different. For plotting purposes, the pushover curves in Fig. 11 are only shown for one event in each centrifuge test. The pushover curves for liquefied conditions exhibit a non-zero displacement at zero shear force due to the application of soil displacements. They also show a softer response as compared to pushover curves for the nonliquefied condition due to softened p-y springs in the liquefied soils and the application of soil displacements. The soil displacements had a more pronounced effect on the pushover curves for liquefied conditions in the cases analyzed in this study due to the fact that flexible piles follow the ground deformations more closely. The variations in p-multipliers had a minor effect on the pushover curves for liquefied conditions, likely because the majority of the piles (except for those in JCB01) were not embedded in liquefied soils.

The equivalent natural period of the soil–wharf system was computed for both conditions in each test using the initial stiffness of the pushover curves and the total wharf mass including the deck and the piles (the deck mass constitutes 74% of the total wharf mass). The effect of initial versus secant stiffness on the equivalent natural period was insignificant. Fig. 12 shows the equivalent natural period of the wharf calculated based on the pushover curves for liquefied and nonliquefied conditions. The wharf natural periods ranged from 0.5 sec to 1 sec in the nonliquefied condition but were elongated to values between 0.8 sec and 1.1 sec in the liquefied condition (an average increase of 25%).

Estimate of Peak Inertia using Equivalent Static Analysis

Equivalent static analyses (ESAs) were performed for liquefied and nonliquefied conditions in order to estimate peak superstructure inertial demands. The pushover curves (Cases A or B) were used to estimate the lateral stiffness and natural period of the wharf system. The acceleration response spectra (ARS) at the ground surface were then used to extract the spectral acceleration at the corresponding natural period of the wharf. The peak inertial load at the wharf deck was estimated by multiplying the spectral acceleration and the wharf mass.

The ESA for nonliquefied conditions included pushover curves (Case A in Fig. 11) combined with the ARS in the lower rock dike, which were representative of a nonliquefied site response. While there were no liquefied soils underlying the lower rock dike, the liquefaction of soils in the backland may have affected the recorded accelerations in the lower rock dike; however, this effect is believed to be minimal. The use of nonliquefied ARS is consistent with procedures proposed by Caltrans (2012), where the peak inertial loads are estimated in the absence of liquefaction and then reduced by 50% to account for the effects of liquefaction on site response and the asynchronous timing of peak inertial and peak kinematic demands.

The ESA for liquefied conditions included a pushover curve (Case B in Fig. 11) combined with an ARS in the backland representative of the accelerations in the liquefied ground. This approach is sometimes used in practice when the effect of liquefaction is already included in the design spectra. It should be noted that the peak inertial demand estimated using this approach will only need to be multiplied by a potential reduction factor due to asynchronous timing of peak inertial and peak kinematic loads. There is considerable damping associated with soil-pile-fluid interaction that should be accounted for in estimating inertial demands. This complex behavior was approximated in the ESA analyses by developing the ARS for 14% damping ratio (as opposed to the typical 5% damping ratio). The equivalent damping ratio of 14% was calculated based on a dashpot coefficient of $c = 4*B*\rho*Vs$ proposed by Wang et al. (1998), where B is the pile diameter and ρ and Vs are the density and shear wave velocity in the rockfill. The damping ratio of 14% provided a reasonable estimate of the peak acceleration at the wharf deck as explained in the next section. For comparison, using 5% damping ratio overestimated the wharf accelerations by a factor of 1.5. Other studies based on centrifuge tests have also shown the importance of accounting for additional damping along the piles to capture the radiation damping and the interaction between soil, structure and fluid and modeled this damping using dashpots along the piles in dynamic analysis (e.g. Shafieezadeh et al. 2012, Brandenberg et al. 2013).

Fig. 13 shows how spectral accelerations were extracted using the ESA approaches described above, using the first event in NJM01 as an example. The natural period of the wharf changed slightly from 0.94 sec in nonliquefied conditions to 0.95 sec in liquefied conditions. The spectral accelerations were calculated from accelerations time histories recorded in the centrifuge test. A black line shows the spectra in the backland that are representative of liquefied conditions; three lines in different shades of blue show the spectra for three different accelerometers in the lower rock dike that are representative of nonliquefied conditions. The base spectra are also shown for comparison purposes. The nonliquefied spectra in the lower rock dike confirm that the lower rock dike moves fairly rigidly and that the extracted spectral acceleration is not sensitive to the location of the selected accelerometer. The spectral acceleration at the natural period of the structure increased from 0.2 g in the nonliquefied condition to 0.24 g in the liquefied condition.

Comparison Between Peak Inertial Demands from Centrifuge Tests and ESA

The accuracy of the ESA methods in estimating inertial demands was evaluated by comparing the estimated peak deck acceleration and peak pile head shear forces with those measured in the centrifuge tests. Fig. 14 shows that ESA for both liquefied and nonliquefied conditions reasonably estimated peak deck accelerations (slightly overestimated by a factor of 1.1.)

The pile head shear in ESA was calculated by distributing the peak deck inertial force (i.e., spectral acceleration multiplied by the wharf mass) between individual piles in the pile group based on their relative lateral stiffness. The pile head shear forces in centrifuge tests were calculated using the measured bending moments from the top two strain gauges in each pile (for piles with two strain gauges located above the ground surface). Fig. 15 shows that the nonliquefied ESA underestimates the measured pile head shear forces by a factor of 0.9, and the liquefied ESA overestimates the measured pile head shear forces by a factor of 1.2. This indicates that the pile head shear forces were, on average, estimated reasonably well. This comparison confirms that no significant bias was introduced in estimating inertial demands that would affect the load combination factors that are proposed next.

Overall, Figs. 14 and 15 show no significant difference between the inertial forces at pile head estimated using ESA for liquefied or nonliquefied conditions. In the subsequent analyses, the liquefied ESA was used to evaluate the accuracy of design methods in estimating pile bending moments. However, it should be noted that performing the ESA for liquefied conditions requires estimation of soil displacement profiles, which includes significant uncertainty and could greatly affect the results for flexible piles. In addition, performing ESA for liquefied conditions requires estimating the response spectra in liquefied soils using effective-stress site response analysis, which also include significant uncertainty. Thus, it is sometimes desirable for design purposes to perform ESA for nonliquefied conditions and the results of this study show that the pile head inertial loads can be reasonably captured using ESA for nonliquefied conditions.

COMBINING PEAK INERTIAL AND PEAK KINEMATIC DEMANDS IN DESIGN

Load Combinations

As the peak inertial and peak kinematic demands do not always occur during the same cycle, Boulanger et al. (2007) recommends combining the peak kinematic demand with a fraction of the peak inertial demand, defined as parameter *Ccc*, which ranged from 0.65 to 0.85 in their investigation. The proposed values in Boulanger et al (2007) were developed primarily for bridge structures with an embedded pile cap and an elevated superstructure. The *Ccc* parameters in this study were calculated for pile-supported wharf structures where the pile cap is rigidly fixed to the superstructure. The back-calculated *Ccc* parameters from the centrifuge tests are described in detail in the companion paper (Souri et al. 202X). The data from this study suggests that *Ccc* decreases as the depth to the maximum pile moment increases, which can be attributed to the finding that the bending moments at the pile head are heavily influenced by, and correlated with, the deck inertia, resulting in *Ccc* values closer to 1. In contrast, the bending moments that develop at depth are less correlated with deck inertia as they are more influenced by kinematic demands and thus will have smaller *Ccc* values.

There is also a noticeable dependence between the *Ccc* values and different soil profiles, as discussed in the companion paper. The *Ccc* values calculated for the first three tests (NJM01, NJM02, and SMS01) range from 0.3 to 0.6, while the *Ccc* values calculated for the last two tests (JCB01 and SMS02) range from 0.9 to 1.0. In the first three tests, the kinematic demands are driven by a large overlying nonliquefiable rockfill. The time-dependent mobilization of slope deformation and corresponding application of kinematic loads on piles associated with this soil profile and configuration resulted in a lower likelihood for the peak kinematic loads to coincide with peak inertial loads. In contrast, the kinematic loads in the last two tests are relatively small and mobilized earlier in the motion. The kinematic loads in JCB01 were driven by a thin layer of rock face underlain by a loose sand layer that liquefied early in the motion and the soil profile in SMS02 did not include a liquefiable layer. The peak kinematic loads in the last two tests were more likely to coincide with peak inertia which resulted in larger *Ccc* values. The difference between the calculated *Ccc* values among different soil profiles highlights the site-specific nature of inertial and kinematic interaction and the subsequent load combination factors.

For the sake of comparison of the tests performed in this study, a *Ccc* value of 85% was used based on the median + 1σ values among all five tests. This multiplier resulted in a better match between the recorded and estimated bending moments in all five tests on average, as presented in the next section. However, it is acknowledged that the scatter in data can be reduced if different inertial load factors are used based on different soil profiles; for example, lower combination factors may be used for soil profiles that resemble those in NJM01, NJM02 and SMS1. Table 2 shows the back-calculated load combinations for different soil profiles. These load combinations were calculated for the soil profile, pile properties, and ground motion considered in the five centrifuge tests in this paper, therefore they are applicable for conditions that are similar to those modeled.

It will be shown in the next section that two uncoupled load combinations were adequate to estimate the bending moments that develop at, and near, the pile head (Case A) and at deep locations (Case C, where depth >10D) in these tests. However, the bending moments at shallow depths (<10D) could only be accurately estimated when the two loads were combined (Case B). Therefore, the inertial multipliers in Table 2 were selected primarily based on the *Ccc* values that were back-calculated for bending moments at shallow locations. Fig. 16 shows a schematic diagram of the ESA load combinations in the p-y analysis. The back-calculated inertial multipliers in Table 2 were used in decoupled, ESA analysis where peak inertial and peak kinematic demands were estimated separately. As suggested in POA (2017) more refined multipliers may be used if nonlinear dynamic analysis is adopted in design.

Comparison of Estimated and Measured Maximum Bending Moments

Equivalent static analyses were performed in *LPILE* using the three load combinations listed in Table 2 and an inertial multiplier of 85% as an average for all tests. The estimated bending moments from the ESA were compared to the measured bending moments in the centrifuge tests. Fig. 17 shows the measured and estimated bending moments for NJM01 Event 11, as an example. The bending moments were compared for key strain gauges where large moments were exhibited during the motion. The large measured bending moments are classified into three categories based on their location: bending moments that develop at the pile head (highlighted in blue in Fig. 17), bending moments that develop shallower than 10D (highlighted in red), and bending moments that develop deeper than 10D (highlighted in green). It was observed that the location of large recorded bending moments varied for different pile rows. In Piles #1, #2 and #3, large bending moments were recorded at the pile head as well as above and below the loose liquefiable layer. This was expected, as the failure shear plane passed through the liquefied layer, imposing significant curvature (and moment) in the piles. In Piles #4, #6, and #7, which did not pass through the loose liquefiable layer, large bending moments were recorded at the pile head and at shallow depths (depths <10D).

The estimated bending moments from ESA using the three load combinations are also shown in Fig. 17. As an example, for Pile #1, it is observed that applying inertia only (indicated by a green line) accurately estimates the measured bending moment at the pile head, while applying kinematics only (indicated by a red line) accurately estimates the measured bending moment at depth. The effects of inertia attenuate within 5 to 6 m from the ground surface (approximately 8 to 10 pile diameters). Fig. 17 also shows that while the p-y analysis may not always accurately capture the location of maximum moments, it is capable of capturing the magnitude of the maximum moment with reasonable accuracy (note the location of the estimated and measured deep bending moments in Pile #1). This analysis was performed for two main shaking events for each of the five tests, producing a total of 10 different experimental results that are used to evaluate the accuracy of the proposed load combinations in estimating the pile bending moments. Similar plots for the other tests are provided in the Supplemental Appendix C.

Plots of the peak bending moments measured in the centrifuge tests and those estimated in the ESA are provided in Fig. 18 for all five tests and two shaking events for each test. In this figure, the dashed lines indicate the mean residual between the estimated and measured values (i.e. residual = *Ln*(estimated/measured)) providing a measure of accuracy for each ESA load combination. At the pile head (Fig. 18a), it can be seen that applying inertia only (Case A) adequately estimated the bending moments (overestimated by +1% on average) while the combined case (Case B) slightly underestimated the bending moments (-9%) and applying kinematics only (Case C) significantly underestimated the bending moments (-95%). This is expected, as pile head bending moments are primarily affected by wharf inertia; thus, it was necessary to apply full inertial load to estimate the demands at this location. For shallow locations (depth <10D) shown in Fig. 18b, a combination of the two loads (Case B) estimated the bending moments with a reasonable accuracy (overestimated by +11%) while applying inertia only (Case A) underestimated the bending moments (-33%) and applying kinematic only (Case C) noticeably underestimated the bending moments (-72%). Note that some shallow bending moments were significantly underestimated using load cases A and C, which makes them inadequate for design. For deep locations with (depth >10D) shown in Fig. 18c, it is clear that applying kinematics only (Case C) overestimated the bending moments (+34%), which is associated with uncertainties in estimating the soil displacement profile. Combining inertia and kinematics (Case B) did not improve the accuracy in estimating deep bending moments (overestimate by 37%) and applying inertia only (Case A) significantly underestimated the bending moments (-95%). Note that the soil displacements in Case C were estimated using Newmark mean values, which were shown to reasonably estimate the permanent soil displacements but underestimate the peak transient soil displacements (Fig. 2). However, this underestimation was compensated by the overestimation of pile curvatures using idealized soil displacement profiles with distinct transitions at layer boundaries. As a sensitivity analysis, combining kinematic demands and full (100%) inertia overestimated the bending moments at pile head by +7%, overestimated the shallow bending moments (depth <10D) by +24%, and overestimated the deep bending moments (depth > 10D) by 37%, on average. While the results presented in Figures 18a to 18c were discussed in the preceding section in terms of average trends between estimated and measured bending moments, there is a noticeably large scatter in the estimated values. This scatter is associated with the inherent limitations in equivalent static analysis where a dynamic, nonlinear response is simplified to a pseudo-static application of loads, as well as the modeling assumptions that were made in these analyses such as the use of a constant inertial multiplier (*Ccc*) of 85% for all tests. This scatter can be reduced by refining the inertial multiplier for each test based on the soil profile and the inertial multipliers reported in Table 2 as guidance. Alternatively, nonlinear dynamic analysis can be performed to refine the combination of inertial and kinematic loads as suggested by POA (2017).

DESIGN EXAMPLE

A design example is presented here to summarize the implementation of the recommended procedure for estimating and combining the inertial and kinematic loads in design. The soil profile and pile properties in Test NJM02 is used in this example. The wharf structure in this example is supported on 21 piles in a 7-by-3 configuration as shown in Figure 1. The pile demands are estimated using the following steps:

Step 1: Estimate kinematic demands:

In this example the lateral soil displacements are estimated using the Newmark sliding block method. The yield acceleration is estimated as 0.053 g using pseudo-static limit equilibrium analysis and is assumed to be constant during the acceleration time histories.

The recorded accelerations from the centrifuge test are used as input for the Newmark analysis; however, in a design project the accelerations are typically obtained from 1D or 2D site response analysis. The mean Newmark displacement at the ground surface is estimated as 0.07 m and is assumed to be distributed linearly with depth in the loose liquefiable layer and to remain constant within the nonliquefiable layers (rockfill and dense sand). The idealized estimated soil profiles along the piles are shown in Figure 3.

Step 2: Estimate peak inertial demands:

The peak inertial loads are estimated in a pseudo-static analysis as described by the following steps.

- Pushover curves are developed in *LPILE* for the entire pile group under the two conditions shown in Figure 10. In the liquefied condition the estimated soil displacements from the previous step is applied to the end nodes of p-y springs and the p-y springs in the liquefiable layer were softened using p-multipliers. The initial lateral stiffness of the wharf-foundation system is estimated as 42,710 kN/m and 42,080 kN/m in nonliquefied and liquefied conditions, respectively (Figure 11). Using the wharf mass of 971.3 Mg, the equivalent natural period is calculated as 0.94 sec and 0.95 sec in nonliquefied and liquefied conditions, respectively. In the following steps in this example, the liquefied condition is used to estimate the peak inertial load.
- The spectral accelerations at the ground surface are calculated from recorded acceleration time histories in the centrifuge test; however, the spectral accelerations are typically developed in design applications based on site-specific site response analysis. The spectral acceleration at the ground surface in the liquefied condition is estimated as PSA = 0.24 g at the structural period of 0.95 sec as shown in Figure 13.

- The total inertial load from the structure mass is calculated as the product of the wharf mass and *PSA* as 971.3 Mg * 0.24 * 9.81 ms^{-2} = 2287 kN. Pile head shear loads are estimated for each pile by distributing the total deck inertial load between the 21 individual piles in the pile group based on their relative lateral stiffness obtained from the pushover analysis.

Step 3: Combine peak inertial and peak kinematic loads to estimate pile demands:

The estimated soil displacement profile and the pile head shear load (multiplied by an inertial load factor, *Ccc*) are imposed in *LPILE* based on the three load combinations shown in Figure 16 and the pile bending moments are estimated accordingly (Figure 17). Table 2 provides some guidance on selecting the inertial load factor (*Ccc*) based on different soil profiles. In this example, a *Ccc* value of 0.85 is used based on the median + 1σ values among all five tests. The comparison of estimated and recorded bending moments in this study showed that applying pile head shear only (Case A) accurately predicts the magnitude of measured bending moments at the pile head, while applying soil displacement only (Case C) accurately estimates the magnitude of recorded bending moments at locations deeper than 10 times pile diameter. Pile bending moments at shallower locations are better estimated when the two loads are combined (Case B).

CONCLUDING REMARKS

The combination of inertial and kinematic demands in pile foundations subjected to liquefaction-induced lateral spreading was investigated using the experimental data from five centrifuge tests on pile-supported wharves in conjunction with a practice-oriented equivalent static analysis using *LPILE*. The peak kinematic demands were estimated from displacement profiles established with the Newmark sliding block method using recorded acceleration time histories in centrifuge tests. The peak inertial demands were estimated using the natural period of the wharf–

foundation system and the spectral acceleration at the ground surface. The analysis was performed for three loading cases: soil displacement only, peak inertia only, and soil displacement combined with 85% of peak inertia. The bending moments estimated from ESA were compared to the peak bending moments measured in the centrifuge tests. The comparison provided a systematic way to evaluate the accuracy of the load combinations in estimating bending moment demands and highlighted circumstances under which each load combination controls the pile design. The primary conclusions of the analyses are summarized as follows.

- Reasonable estimates of bending moments at the pile head were made by applying only the peak inertial load, while bending moments at deep locations (>10D) were overestimated by 34% by applying only the kinematic demands.
- Bending moments at shallow locations (<10D) were reasonably estimated (overestimated by 11%) by combining kinematic demands with 85% of peak deck inertial load.
- Median soil displacements calculated using the Newmark sliding block method were well correlated with permanent, residual displacements from the centrifuge tests, but underestimated the peak transient displacements. Newmark median + 1σ values were better correlated with the peak transient displacements from the centrifuge tests.
- There is considerable uncertainty in predicting the pattern of soil displacement with depth, and this significantly affects the estimated bending moments in the equivalent static analysis of flexible piles. The idealized profile of soil displacements in multi-layered soils based on the maximum shear strain potential in each layer (i.e. LDI approach) resulted in distinct transitions. In the cases that were analyzed in this study, the overestimation of bending moments due to distinct transitions in idealized soil displacement profiles appeared to cancel out the underestimation of peak transient soil displacements using the Newmark mean values. A more

rigorous analysis may include smoothening the transition over one to two pile diameters, as recommended by Caltrans (2012) and McGann et al. (2011), combined with the use of peak transient displacements.

- The peak deck accelerations and the peak shear forces at pile head were reasonably estimated by ESA methods using pushover analyses for both liquefied and nonliquefied conditions.
- The analyses in this study suggest that higher damping ratios (> 5%) may be warranted in estimating deck accelerations to approximate the combined influence of radiation damping, nonlinear soil behavior and inelastic pile performance consistent with the cyclically-induced permanent deformations.
- The portion of the peak inertia that was acting at the deck during the critical cycle (*Ccc*) ranged from 0.2 to 1.0 and appeared to be generally correlated with soil profile and the dynamic response of each soil unit. The five tests were subdivided into two general categories: Profile B1 is characterized as configurations that include deep-seated liquefaction underlying significant nonliquefiable crust (i.e. rockfill). Profile B2 is characterized as configurations that include generally smaller kinematic demands associated with either nonliquefiable profiles or weak/softened soils closer to the ground surface, and thin nonliquefiable crust (i.e. sliver rockfill). Inertial multipliers (*Ccc*) of 0.3 to 0.6 were back-calculated for soil profiles that resemble Profile B1 and *Ccc* values of 0.9 to 1.0 were back-calculated for soil profiles that resemble Profile B2.
- The wide range of *Ccc* values observed in this research highlights the need for sensitivity analysis when performing ESA, and the benefit of performing coupled nonlinear dynamic analysis that capture complex soil-pile-structure interaction for varying soil profiles.

- The load combination factors were used in this study in decoupled analysis using the p-y spring approach and are not necessarily appropriate for use with the simplified equivalent fluid pressure for lateral spreading load.

These conclusions are applicable only for relatively flexible piles with small diameters (up to about 0.7 m). The interaction of inertial and kinematic loads could be different for pile shafts with larger diameters. Incorporating uncertainties in design (e.g. uncertainties associated with estimating ground motions) may introduce bias in estimating inertial demands that could affect how the inertial and kinematic demands are combined. The sensitivity of the proposed load combinations to these uncertainties is an important issue that needs to be evaluated in future studies.

DATA AVAILABILITY STATEMENT

Some or all data, models, or code generated or used during the study are available at the Center of Geotechnical Modeling at the University of California at Davis (https://cgm.engr.ucdavis.edu) in accordance with granting agency data retention policies.

ACKNOWLEDGEMENTS

Support for centrifuge testing was provided by the National Science Foundation (Grant No. CMS-9702744) and the Pacific Earthquake Engineering Research Center (Grant No. SA2394JB) [Dickenson, P.I.]. Support for the recent analysis of the test results was provided by the National Science Foundation (Grant No. CMMI-1761712) and the Deep Foundations Institute (Grant No. 171126) [Khosravifar, P.I.]. Any opinions, findings, and conclusions or recommendations expressed in this material are those of the author(s) and do not necessarily reflect the views of the funding agencies.

SUPPLEMENTAL DATA

Supplemental Appendix A provides details on the calibration of the *LPILE* models using four quasi-static lateral load tests. Supplemental Appendix B provides input parameters used in the Newmark sliding block analyses. Supplemental Appendix C shows the comparison between measured and estimated bending moments for all five centrifuge tests (NJM01, NJM02, SMS01, SMS02 and JCB01). The supplemental appendices are available online in the ASCE Library (www.ascelibray.org).

REFERENCES

AASHTO (American Association of State Highway and Transportation Officials). 2014. *Guide Specifications for LRFD Seismic Bridge Design*. 2nd ed. with 2014 Interim. Washington, DC: AASHTO.

Abdoun, T., and R. Dobry. 2002. "Evaluation of pile foundation response to lateral spreading." *Soil Dyn. and Earthq. Eng.* 22: 1051–1058. https://doi.org/10.1016/S0267-7261(02)00130-6.

Abdoun, T., Dobry, R., O'Rouke, T. D., and S. H. Goh. 2003. "Pile response to lateral spreads: Centrifuge modelling." *J. Geotech. Geoenviron. Eng*. 129(10): 869–878. https://doi.org/10.1061/(ASCE)1090-0241(2003)129:10(869).

American Petroleum Institute, API, 1993. Recommended practice for planning, design, and constructing fixed offshore platforms. API RP 2A–WSD, 20th Ed., API, Washington, D.C.

Armstrong, R. J., R. W. Boulanger, and M. H. Beaty. 2014. "Equivalent static analysis of piled bridge abutments affected by earthquake-induced liquefaction." *J. Geotech. Geoenviron. Eng.* 140 (8): 04014046. https://doi.org/10.1061/(ASCE)GT.1943-5606.0001152

ASCE (American Society of Civil Engineers). 2014. *Seismic Design of Piers and Wharves*. *ASCE/COPRI 61-14.* Reston, VA: ASCE Standards Committee on Seismic Design of Piers and Wharves. https://doi.org/10.1061/9780784413487

Ashford, S., Boulanger, R., and Brandenberg, S. 2011. "Recommended Design Practice for Pile Foundations in Laterally Spreading Ground." Report PEER 2011/04, Pacific Earthquake Engineering Research Center (PEER), Berkeley, CA.

Brandenberg, S. J., R. W. Boulanger, B. L. Kutter, and D. Chang. 2007. "Static pushover analyses of pile groups in liquefied and laterally spreading ground in centrifuge tests." *J. Geotech. and Geoenviron. Eng.* 133 (9): 1055–1066. https://doi.org/10.1061/(ASCE)1090-0241(2007)133:9(1055)

Boland, C. B., S. M. Schlechter, N. J. McCullough, S. E. Dickenson, B. L. Kutter, and D. W. Wilson. 2001a. *Pile-Supported Wharf — Centrifuge Model SMS02. Report No. GEG04-2000.* Oregon State University/University of California at Davis.

Boland, C.B., S. M. Schlechter, N. J. McCullough, S. E. Dickenson, B. L. Kutter, and D.W. Wilson. 2001b. *Pile-Supported Wharf — Centrifuge Model JCB01. Report No. GEG05-2000*. Oregon State University/University of California at Davis.

Boulanger, R. W., Curras, C. J., Kutter, B. L., Wilson, D. W., & Abghari, A. 1999. "Seismic soil-pile-structure interaction experiments and analyses." *Journal of geotechnical and geoenvironmental engineering*, *125*(9), 750-759.

Boulanger, R. W., D. Chang, S. J. Brandenberg, R. J. Armstrong, and B. L. Kutter. 2007. “Seismic design of pile foundations for liquefaction effects.” In *Proc. of 4th International Conf. on Earthq. Geotech. Eng.*, 277–302. Dordrect, Germany: Springer. https://doi.org/10.1007/978-1-4020-5893-6_12

Brandenberg, S. J., Boulanger, R. W., Kutter, B. L., and D. Chang. 2007. “Static pushover analyses of pile groups in liquefied and laterally spreading ground in centrifuge tests.” *J. Geotech. Geoenviron. Eng.* 133 (9): 1055–1066. https://doi.org/10.1061/(ASCE)1090-0241(2007)133:9(1055).

Brandenberg, S. J., Zhao, M., Boulanger, R. W., & Wilson, D. W. 2013. “p-y plasticity model for nonlinear dynamic analysis of piles in liquefiable soil.” *Journal of geotechnical and geoenvironmental engineering*, *139*(8), 1262-1274.

Broms, B.B. 1964. "Lateral Resistance of Piles in Cohesionless Soils." Journal of the Soil Mechanics and Foundations Division. American Society of Civil Engineers. Vol 90, No. SM3, May, 1964. pp 123-157

Caltrans (California Department of Transportation). 2012. *Guidelines for Foundation Loading and Deformation Due to Liquefaction Induced Lateral Spreading*. Sacramento, CA: Caltrans.

Caltrans (California Department of Transportation). 2016. *Bridge Memo to Designer (MTD) 20-4: Seismic Retrofit Guidelines for Bridges in California*. Sacramento, CA: Caltrans.

Chang, D., 2007. “Seismic Performance of Pile-Supported-Structures in Liquefied and Laterally Spreading Ground*.” Ph.D. Thesis,* University of California, Davis

Cubrinovski, M., Winkley, A., Haskell, J., Palermo, A., Wotherspoon, L., Robinson, K., Bradley, B., Brabhaharan, P. and Hughes, M., 2014. “Spreading-induced damage to short-span bridges in Christchurch, New Zealand.” *Earthquake Spectra*, *30*(1), pp.57-83.

Cubrinovski, M., Bray, J. D., de la Torre, C., Olsen, M. J., Bradley, B. A., Chiaro, G., Stocks, E. and L. Wotherspoon. 2017. “Liquefaction effects and associated damages observed at the Wellington Centreport from the 2016 Kaikoura earthquake.” *Bull. N. Z. Soc. Earthq. Eng*., 50 (2): 152–173.

Dickenson, S., Yang, S., Schwarm, D., & Rees, M. 2016. “Design Considerations for the Kinematic Loading of Piles.” In *Proc. Ports 2016 Conference* (pp. 213-222).

Dobry, R., Abdoun, T., O’Rourke, T. D., and S. H. Goh. 2003. “Single piles in lateral spreads: Field bending moment evaluation.” *J. Geotech. Geoenviron. Eng.* 129, 879–889. https://doi.org/10.1061/(ASCE)1090-0241(2003)129:10(879)

Donahue, M. J., Dickenson, S. E., Miller, T.H., and Yim, S.C. (2005). “Implications of the Observed Seismic Performance of a Pile Supported Wharf for Numerical Modeling.” Earthquake Spectra, EERI, 21(3), 617-634.

Ebeling, R. M., and E. E. Morrison, Jr. 1992. *The Seismic Design of Waterfront Retaining Structures. Tech. Rep. No. ITL-92-11*. Port Hueueme, CA: U.S. Naval Civil Engineering Lab.

Hamada, M., Yasuda, S., Isoyama, R., and Emoto, K. 1986. ‘‘Study on liquefaction induced permanent ground displacements.’’ Research Rep., Association for Development of Earthquake Prediction, Japan, November, 87.

Idriss, I. M., and Boulanger, R. W., 2008. “Soil Liquefaction During Earthquakes,” EERI MNO-12, Earthquake Engineering Research Institute, Oakland, CA.

Kramer, S.L. 2008. “Evaluation of Liquefaction Hazards in Washington State.” Washington State Department of Transportation (WSDOT), WA-RD 668.1.

Liu, L., and R. Dobry. 1995. “Effect of liquefaction on lateral response of piles by centrifuge model tests.” *NCEER Bulletin* 91: 7–11.

LPILE. 2016. “LPILE: A program for the analysis of piles and drilled shafts under lateral loads.” Version 2016.9.10 [computer program]. Austin, Texas: Ensoft Inc.

McCullough, N.J., S.E. Dickenson, B. L. Kutter, and D.W. Wilson. 2000. *Pile-Supported Wharf — Centrifuge Model NJM01. Report No. GEG01-2000*. Oregon State University/University of California at Davis.

McCullough, N. J., S. E. Dickenson, and S. M. Schlechter. 2001. “The seismic performance of piles in waterfront applications.” In *Ports Conference 2001*, 1–10. Reston, VA: ASCE. https://doi.org/10.1061/40555(2001)83

McCullough, N., and S. Dickenson. 2004. “The Behavior of Piles in Sloping Rock Fill at Marginal Wharves.” In *Proc. Ports Conference 2004*, Reston, VA: ASCE. https://doi.org/10.1061/40727(2004)86

McCullough, N. J. 2004. “The seismic geotechnical modeling, performance, and analysis of pile-supported wharves.” Oregon State University.

McCullough, N. J., S. E. Dickenson, and S. M. Schlechter. J. C. Boland 2007. “Centrifuge Seismic Modeling of Pile-Supported Wharves.” Geotechnical Testing Journal, Vol. 30, No. 5

MCEER (Multidisciplinary Center for Earthquake Engineering Research). 2003. *Recommended LRFD Guidelines for the Seismic Design of Highway Bridges.* MCEER/ATC-49, Report No. MCEER-03-SP03. Buffalo, N.Y.: University at Buffalo.

McGann, R., P. Arduino, and P. Mackenzie-Helnwein. 2011. “Applicability of conventional p–y relations to the analysis of piles in laterally spreading soil.” *J. Geotech. Geoenviron. Eng.* 137 (6): 557–567. https://doi.org/10.1061/(ASCE)GT.1943-5606.0000468

Newmark, N.M. 1965. “Effects of Earthquakes on Dams and Embankments.” *Geotechnique* 15 (2): 139–160. https://doi.org/10.1680/geot.1965.15.2.139

ODOT (Oregon Department of Transportation). 2014. *Geotechnical Design Manual*. Salem, OR: ODOT Technical Services Branch.

Olson, S.M., Hashash, Y.M.A., Muszynski, M.R., and Phillips, C. 2017. “Passive wedge formation and limiting lateral loads on large foundations during lateral spreading.” ASCE Journal of Geotechnical and Geoenvironmental Engineering, 143(7), 13p

POLB (Port of Long Beach). 2015. “Port of Long Beach Wharf Design Criteria,” Version 4.0 (May). Long Beach, CA: POLB.

POA (Port of Anchorage) 2017. “Anchorage Port Modernization Project Seismic Design Manual”.

Rathje, E., Bachhuber, J., Cox, B., French, J., Green, R., Olson, S., Rix, G., Wells, D., and Suncar, O. 2010. “Geotechnical engineering reconnaissance of the 2010 Haiti earthquake.” GEER Association, Report No. GEER-021.

Schlechter, S. M., N. J. McCullough, S. E. Dickenson, B. L. Kutter, and D. W. Wilson. 2000a. *Pile-Supported Wharf — Centrifuge Model NJM02. Report No. GEG02-2000*. Oregon State University/University of California at Davis.

Schlechter, S. M., N. J. McCullough, S. E. Dickenson, B. L. Kutter, and D. W. Wilson. 2000b. *Pile-Supported Wharf — Centrifuge Model SMS01. Report No. GEG03-2000*. Oregon State University/University of California at Davis.

Seed, R. B, and Harder, L. F., 1990. “SPT-based analysis of cyclic pore pressure generation and undrained residual strength,” in *Proceedings, Seed Memorial Symposium,* J. M. Duncan, ed., BiTech Publishers, Vancouver, British Columbia, pp. 351–76.

Shafieezadeh, A., DesRoches, R., Rix, G. J., & Werner, S. D. (2012). “Seismic performance of pile-supported wharf structures considering soil-structure interaction in liquefied soil.” *Earthquake Spectra*, *28*(2), 729-757.

Souri, M., A. Khosravifar, S. Schlechter, N. McCullough, and S. E. Dickenson. 2019. "Seismic Performance of Pile-Supported Piers and Wharves Subjected to Foundation Deformations" In *PORTS '19*. Reston, VA: ASCE. https://doi.org/10.1061/9780784482612.058

Souri, M., A. Khosravifar, S. Schlechter, N. McCullough, and S. E. Dickenson. 2020. "Development of experimental p-y curves from centrifuge tests for piles subjected to static loading and liquefaction-induced lateral spreading." *DFI Journal*, 14(1): 1-15.

Souri, M., A. Khosravifar, S. E. Dickenson, S. Schlechter, and N. McCullough. 2022. "Pile-supported wharves subjected to inertial loads and lateral ground deformations: observations from centrifuge tests." (companion paper)

Stark, T. D., & Mesri, G. 1992. "Undrained shear strength of liquefied sands for stability analysis. *Journal of Geotechnical Engineering*," *118*(11), 1727-1747.

Tokimatsu, K., and Y. Asaka. 1998. "Effects of liquefaction-induced ground displacements on pile performance in the 1995 Hyogoken-Nambu earthquake." *Soils Found.* 38 (suppl.): 163–177.

Tokimatsu, K., Suzuki, H., and M. Sato. 2005. "Effects of inertial and kinematic interaction on seismic behavior of pile with embedded foundation." *Soil Dyn. Earthq. Eng.* 25 (7–10): 753–762. https://doi.org/10.1016/j.soildyn.2004.11.018

Turner, B. J., Brandenberg, S. J., and J. P. Stewart. 2016. "Case study of parallel bridges affected by liquefaction and lateral spreading." *J. Geotech. Geoenviron. Eng.* 142.7 (2016): 05016001.

Wang, S., Kutter, B. L., Chacko, J., Wilson, D. W., Boulanger, R. W., and Abghari, A. 1998. "Nonlinear seismic soil-pile-structure interaction." Earthquake Spectra, Earthquake Engineering Research Institute, 14(2), 377-396.

Wilson, D. W. 1998. "Soil–pile–superstructure interaction at soft and liquefying soil sites." *Davis California: University of California*.

Wright, S.G., 1992. UTEXAS3, A Computer Program for Slope Stability Calculations. Austin, Texas. May, 1990, revised July 1991 and 1992.

WSDOT (Washington Dept. of Transportation) 2021. Geotechnical Design Manual. M 46-03.14. Olympia, WA: WSDOT.

Zhang, G., Robertson, P. K., and Brachman, R. W. I., 2004. "Estimating liquefaction-induced lateral displacements using the standard penetration test or cone penetration test," J. Geotech. Geoenviron. Engrg., ASCE, 130, 861–871.

LIST OF TABLES

LIST OF FIGURES

Table 1. Design guidelines on combination of inertial and kinematic demands on piles

Design Code	Recommendation
ASCE 61-14 (2014) Section C4.7 and Port of Long Beach Wharf Design Criteria (POLB 2015)	Locations of maximum bending moment from inertial and lateral ground deformation are spaced far enough apart that the two loads do not need to be superimposed. Maximum bending moments occur at different times. The two loads should be treated uncoupled for marginal wharves.
Port of Anchorage Modernization Program Seismic Design Manual (POA 2017)	Combine peak inertial loading from earthquake ground motion with 100% peak kinematic demands from lateral ground displacements. Smaller factors are allowed if peer-reviewed 2-D nonlinear numerical analysis is used (no less than 25%).
AASHTO (2014)	Design the piles for the simultaneous effects of inertial and lateral spreading loads only for large magnitude earthquakes (M>8).
MCEER/ATC (2003)	For most earthquakes, peak inertia is likely to occur early in the ground motion. Design piles for independent effects of inertia and lateral spreading. For large magnitude and long-duration earthquakes the two loads may interact.
PEER (2011)	100% kinematic + (65% to 85%) inertial (multiplied by 0.35 to 1.4 to account for the effects of liquefaction on peak inertial load)
Caltrans (2012) and ODOT (2014)	100% kinematic + 50% inertial
WSDOT (2021)	100% kinematic + 25% inertial

Table 2. Back-calculated load combinations to combine inertial load and kinematic load from lateral ground deformations for the centrifuge tests in this study

(Case) Load combination	Portion of permanent soil displacements applied at end nodes of p-y springs[1]	Portion of peak deck inertial force applied at deck[2]	Applicability
(A) Inertia only	NA	100%	Adequate to estimate bending moments at pile head.
(B1) Combined kinematic and inertial demands-Profile B1[3]	100%	0.3 to 0.6[5]	Suitable to estimate bending moments below grade down to depth of 10D.
(B2) Combined kinematic and inertial demands-Profile B2[4]	100%	0.9 to 1.0[5]	Suitable to estimate bending moments below grade down to depth of 10D.
(C) Kinematic only	100%	NA	Adequate to estimate pile bending moments deeper than 10D.

1. Soil displacement profiles in this study were estimated using the mean Newmark values distributed with depth using an idealized profile based on the lateral displacement index approach (Zhang et al. 2004; Idriss and Boulanger 2008)
2. Peak deck inertial forces were estimated in this study using ESA performed for liquefied conditions. If ESA is performed for nonliquefied conditions, an additional multiplier may be needed (*Cliq* per Boulanger et al. 2007) to account for the effects of liquefaction on the wharf peak inertial demands.
3. Profile B1 represents typical cross sections in tests NJM02, NJM02, and SMS01 which can be characterized as configurations that include deep-seated liquefaction underlying significant nonliquefiable crust (i.e. rockfill).
4. Profile B2 represent the cross sections in two tests that can be characterized as configurations that include generally smaller kinematic demands/loads associated with either nonliquefiable profile (test SMS02) or weak/softened soils closer to the ground surface, and thin nonliquefiable crust (test JCB01).
5. These ranges provide an initial baseline for preliminary analysis subject to refinement on a project-specific basis. The load combination factors presented here are appropriate for decoupled analysis using the p-y spring approach and are not necessarily appropriate for use with the simplified equivalent fluid pressure for lateral spreading load.

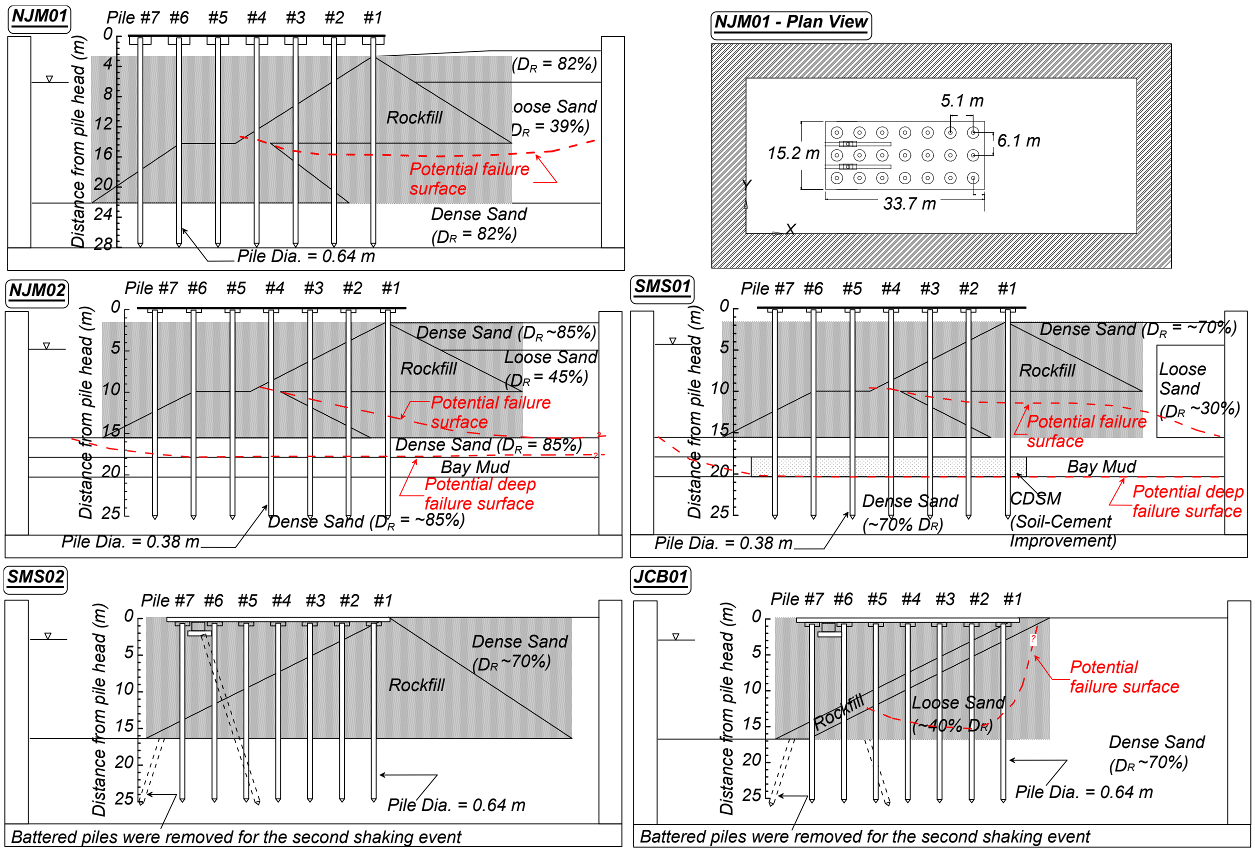

Fig. 1. Cross sections and plan view of five centrifuge tests on pile-supported wharves.

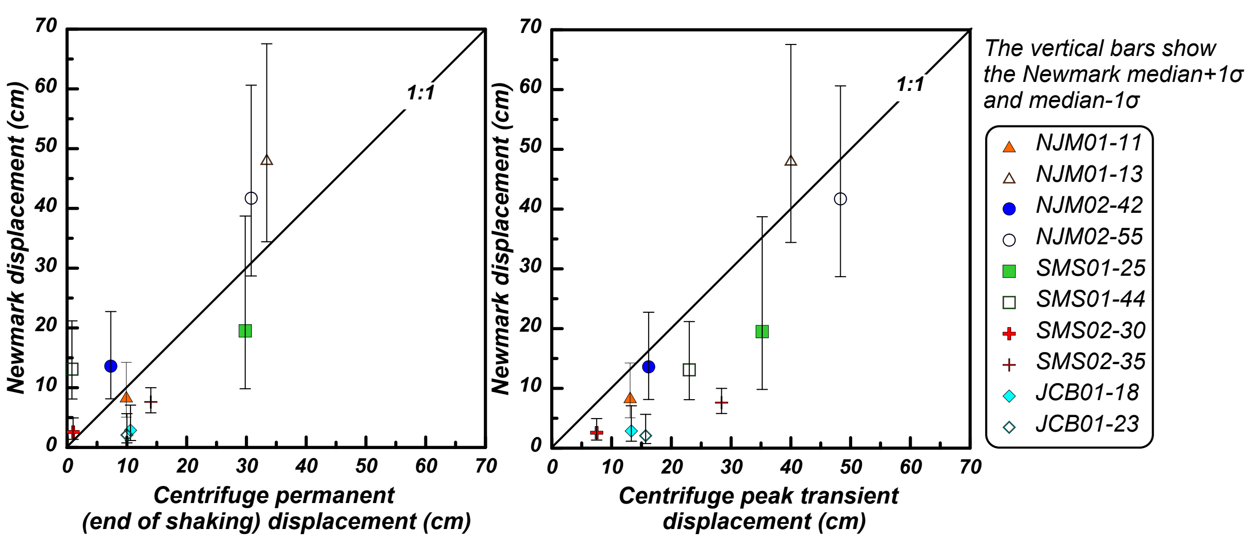

Fig. 2. Comparison of estimated and measured ground surface soil displacements.

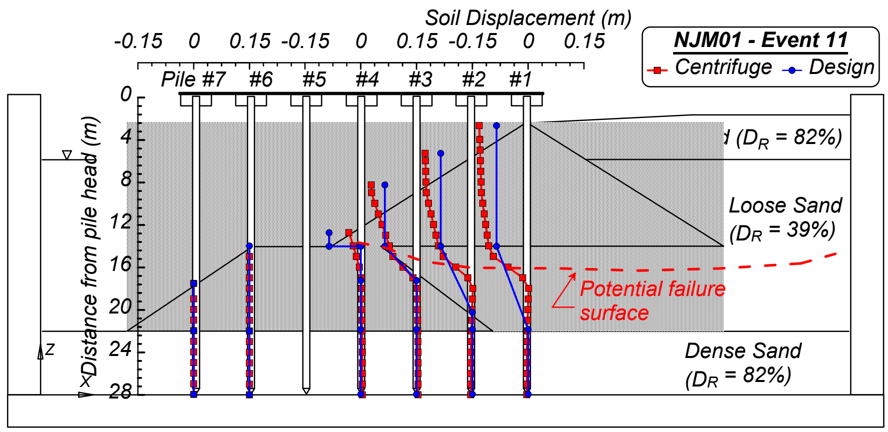

Fig. 3. Comparison of soil displacements at pile locations estimated in design (mean Newmark) and interpreted from centrifuge test results (peak transient) for NJM01 Event 11.

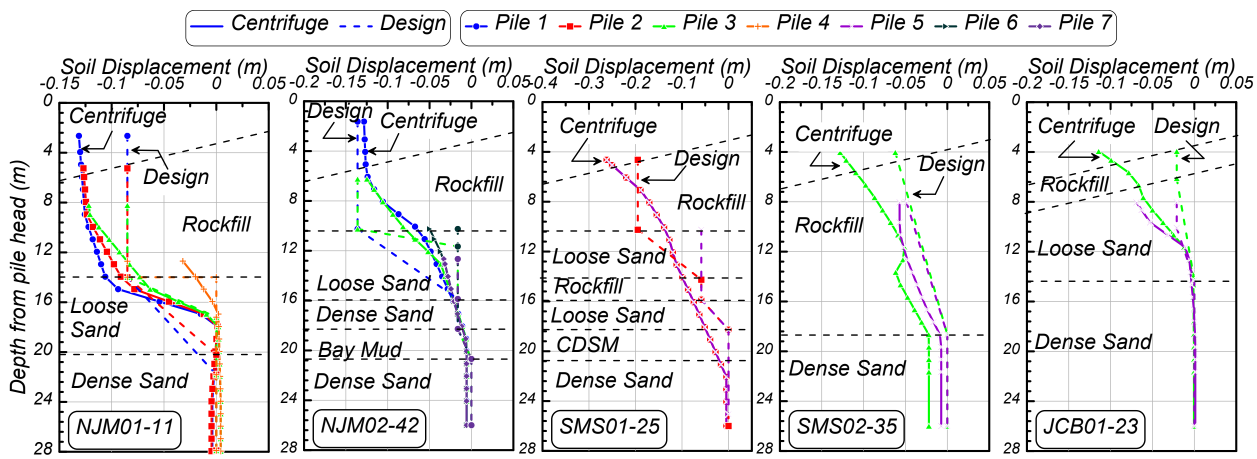

Fig. 4. Comparison of soil displacement profiles at the pile locations interpreted from centrifuge tests (peak transient) and estimated in design (mean Newmark).

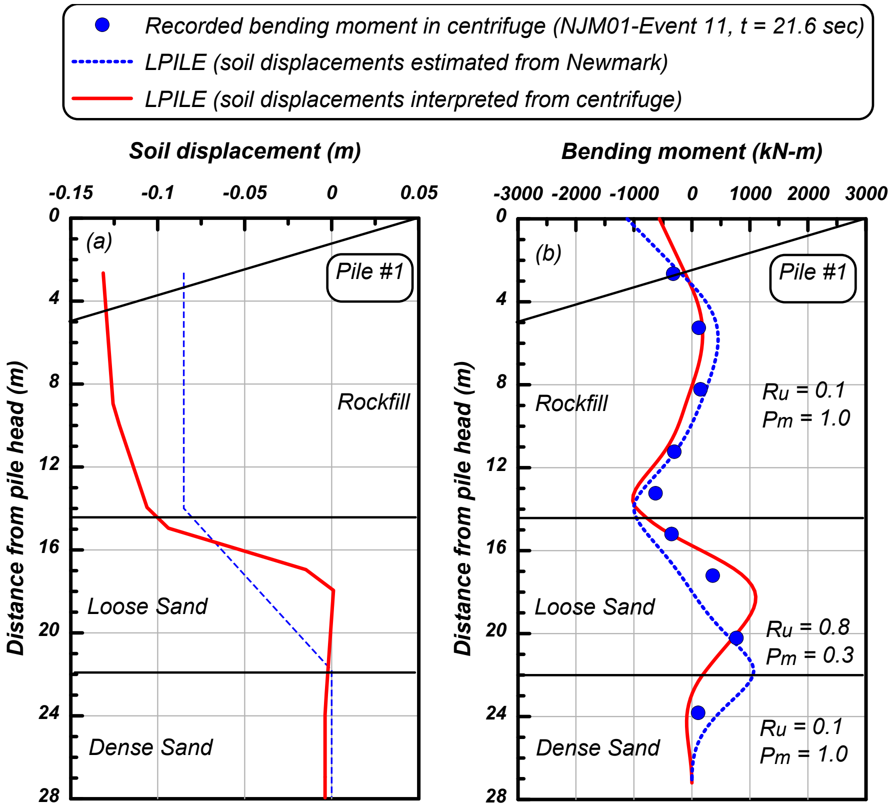

Fig. 5. (a) Comparison of soil displacement profiles interpreted from centrifuge test (peak transient) and estimated in design (mean Newmark) for Pile #1 in NJM01. (b) comparison of estimated bending moments from *LPILE* and measured bending moments from centrifuge

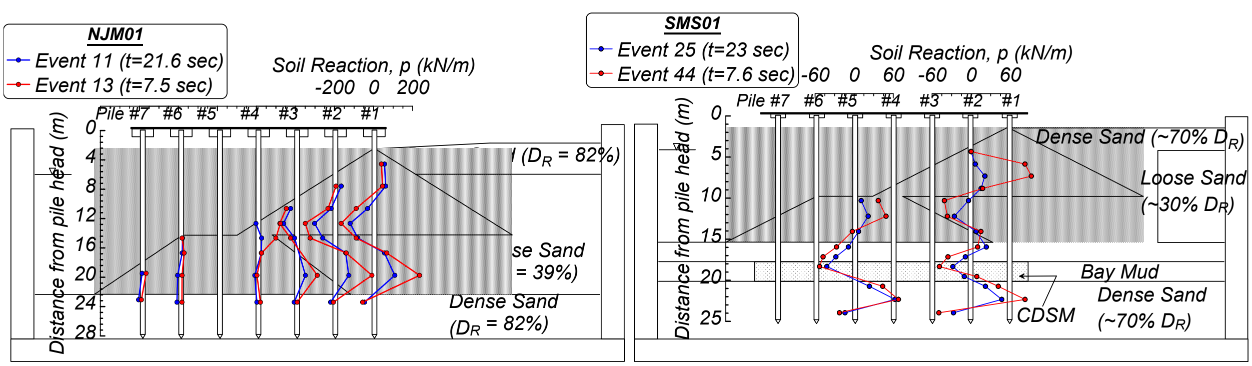

Fig. 6. Soil reaction profiles at the time of maximum bending moment in NJM01 and SMS01.

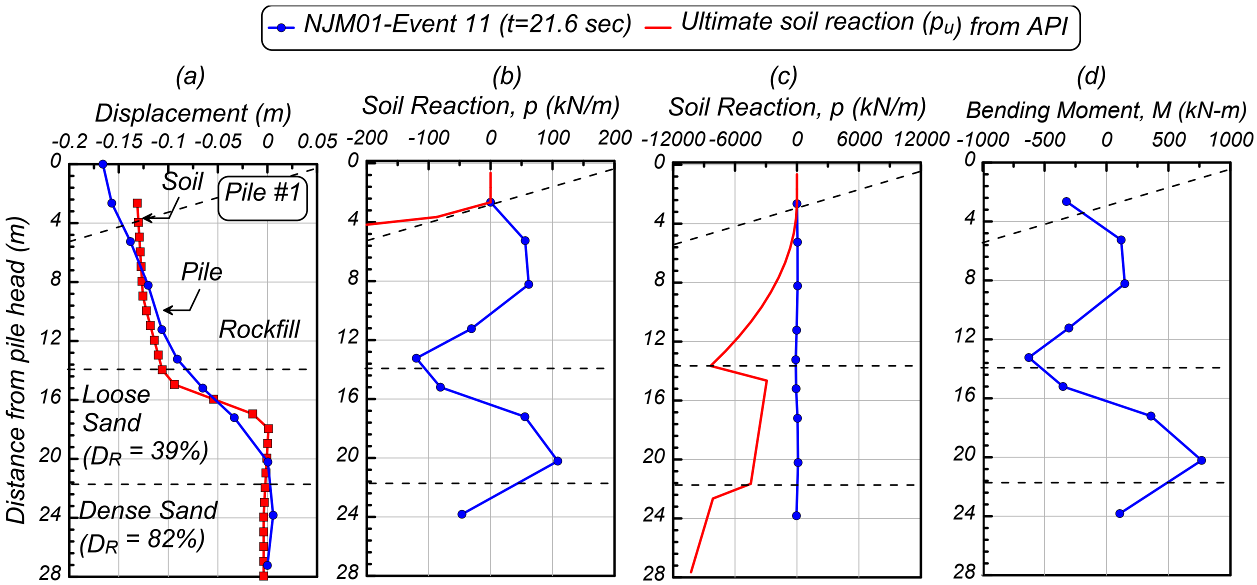

Fig. 7. (a) Displacement, (b) soil reaction at small scale, (c) soil reaction at large scale, and (d) bending moment profiles at the time of maximum bending moment for Pile 1 in NJM01 Event 11.

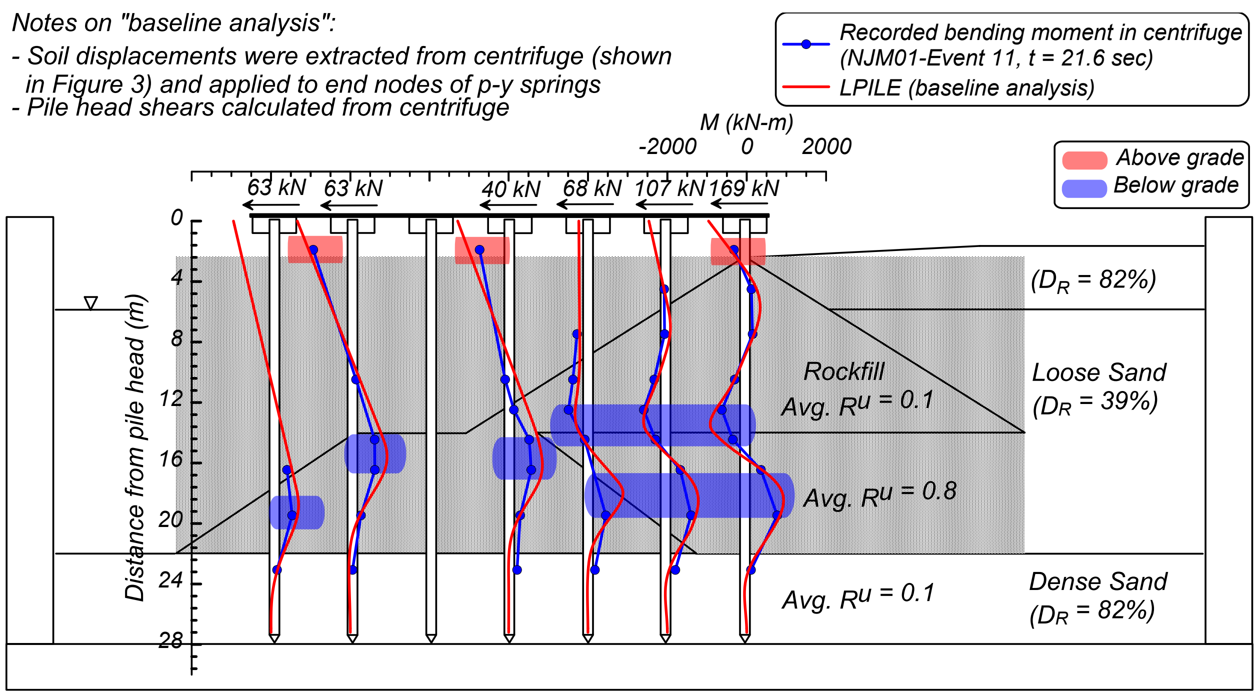

Fig. 8. Comparison of recorded maximum bending moments for all instrumented piles in NJM01 Event 11 with estimated values from the baseline analysis in *LPILE*

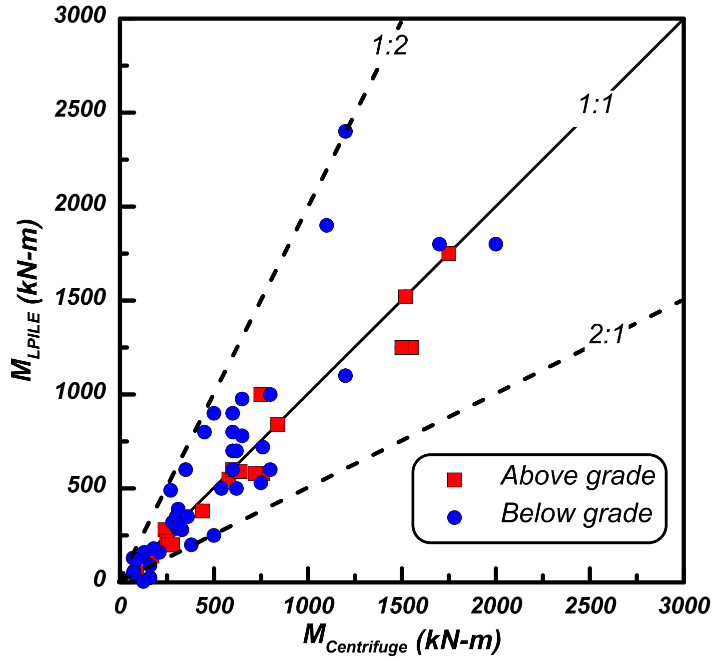

Fig. 9. Comparison of maximum bending moments recorded from centrifuge and predicted from *LPILE* baseline analyses (soil displacements and pile head shear extracted from centrifuge) for all five centrifuge tests

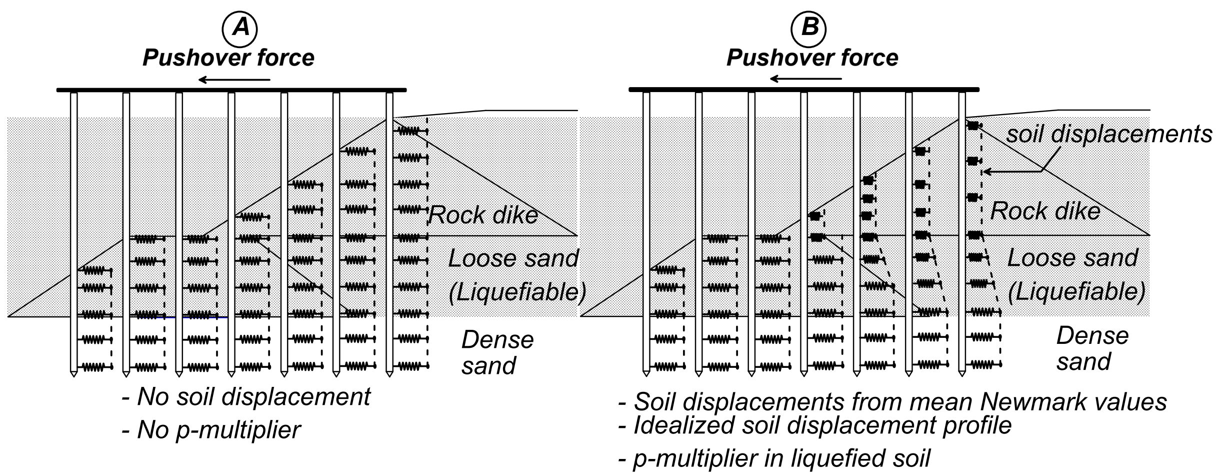

Fig. 10. Schematic of (a) nonliquefied and (b) liquefied pushover analyses.

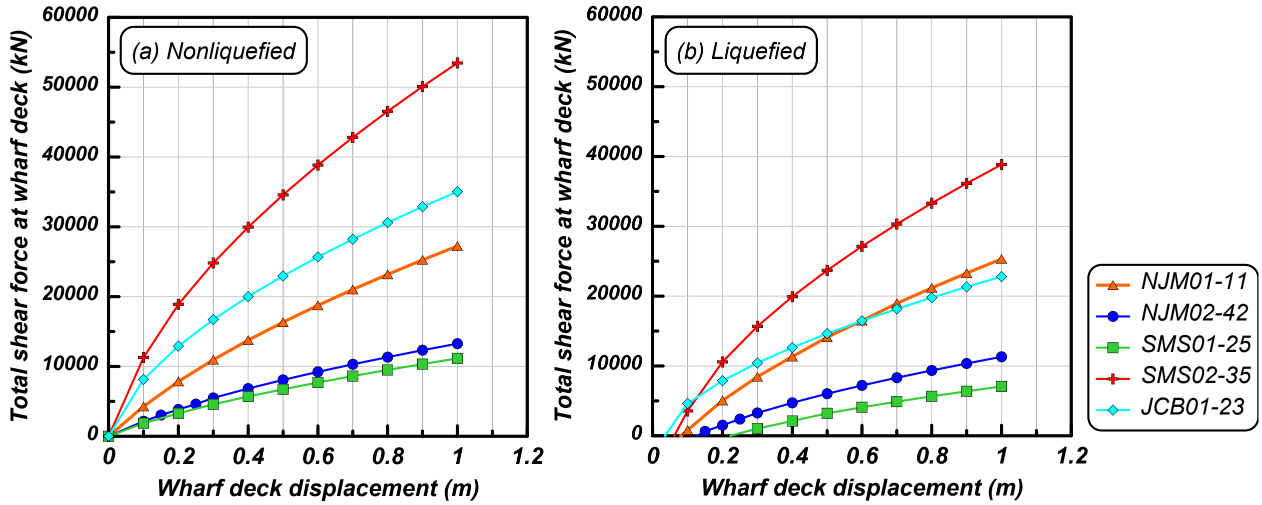

Fig. 11. Pile group force–displacement relationships (pushover curves) for nonliquefied and liquefied conditions.

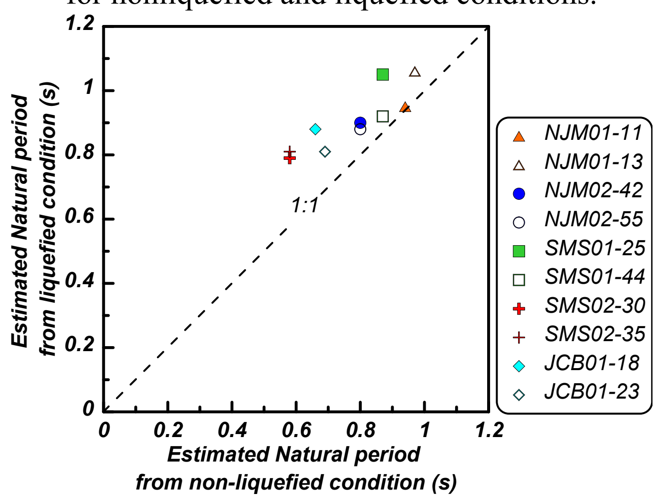

Fig. 12. Comparison of estimated natural period in liquefied condition against nonliquefied condition from pushover analyses.

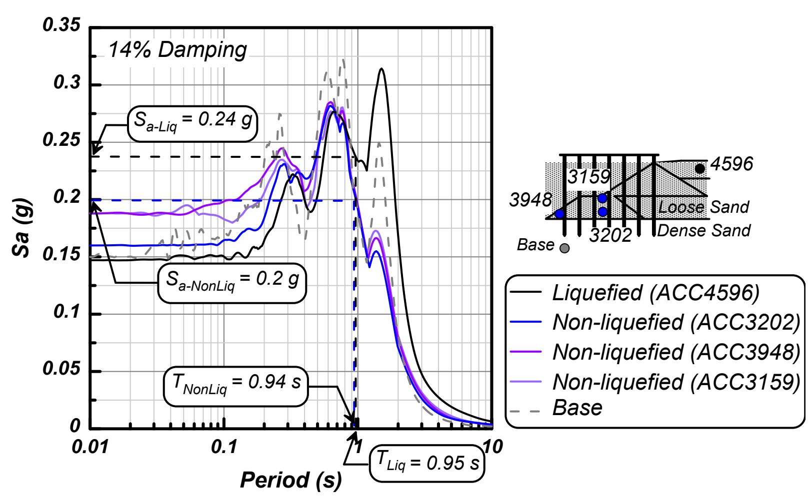

Fig. 13. Spectral accelerations for liquefied and nonliquefied conditions for NJM01 Event 11.

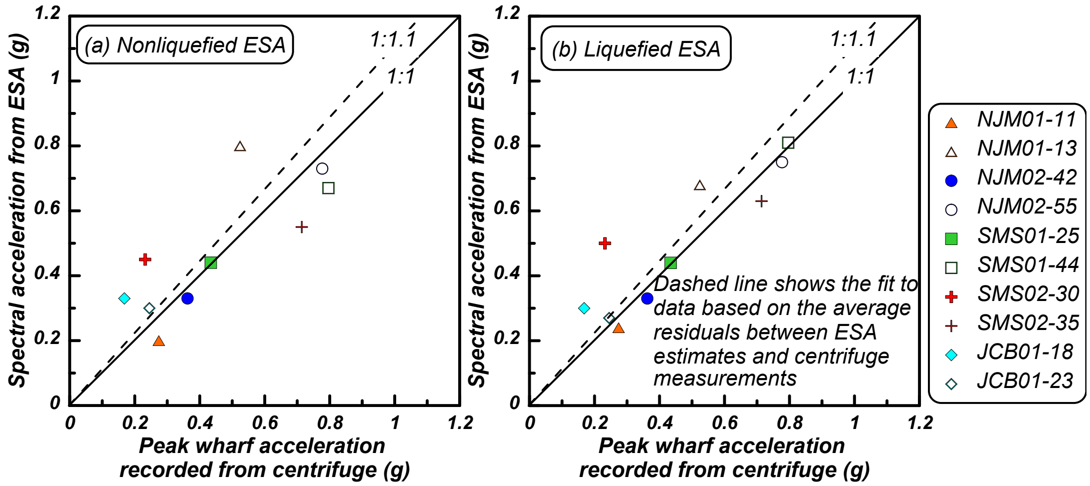

Fig. 14. Comparison of estimated spectral acceleration from design method to peak wharf acceleration measured in the centrifuge tests.

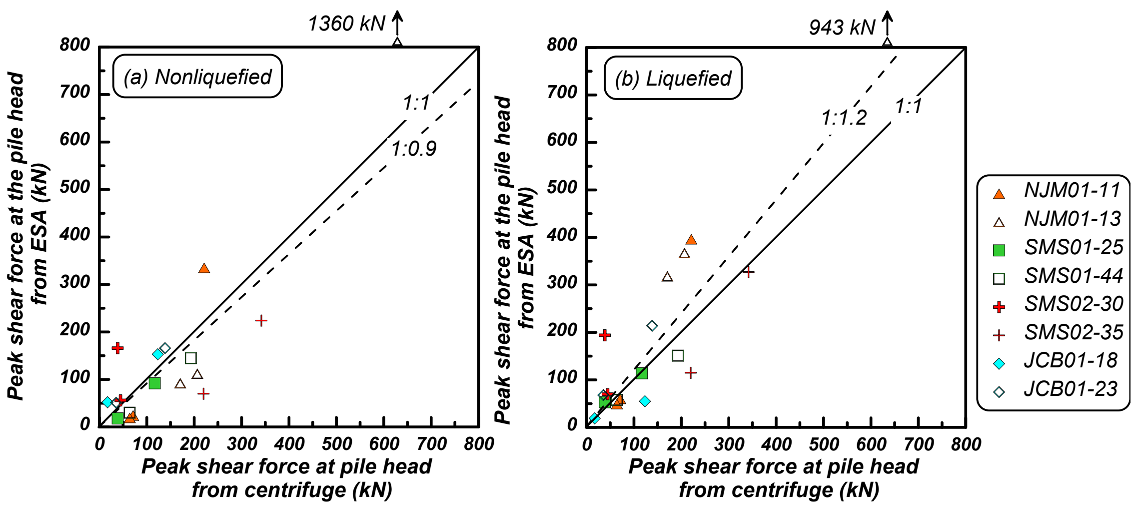

Fig. 15. Comparison of estimated shear force from pushover analysis to the peak shear force at the pile head calculated from the centrifuge test results.

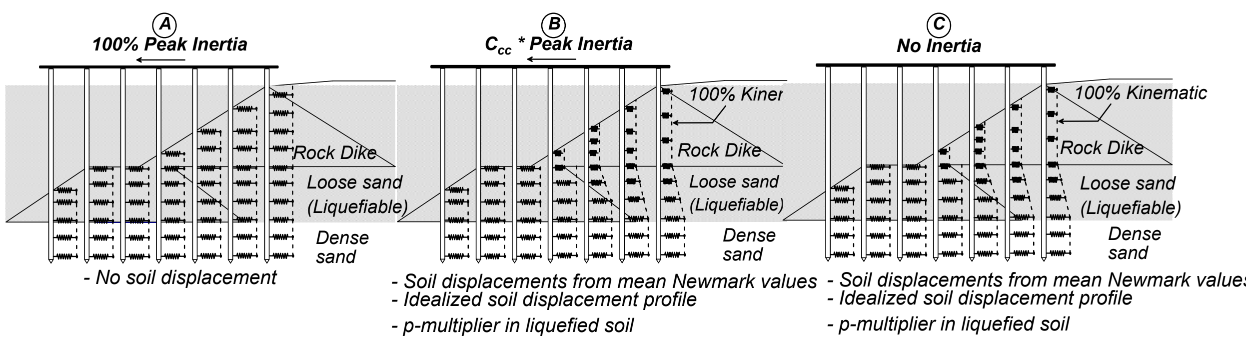

Fig. 16. Schematic of proposed ESA load combinations for piles subjected to ground deformations: (a) inertia only, (b) combined inertia and kinematic, and (c) kinematic only.

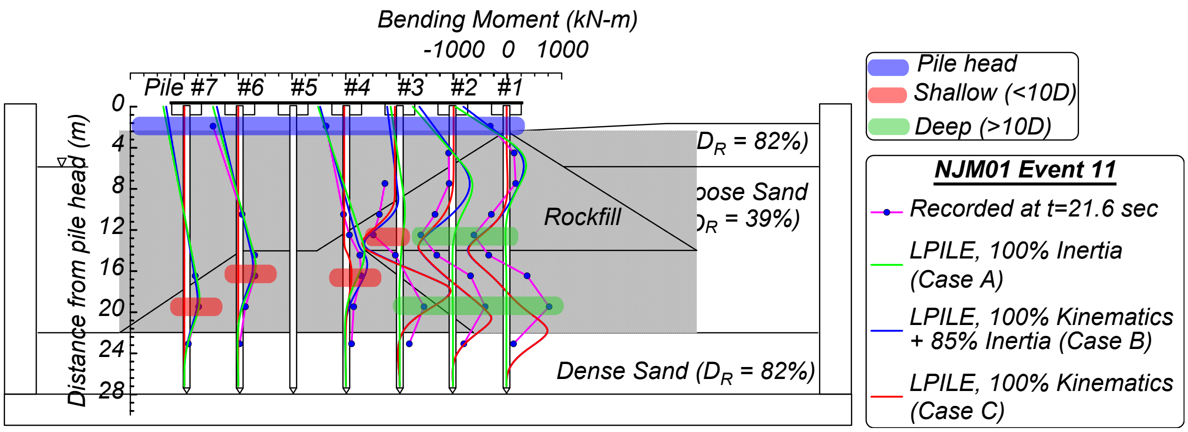

Fig. 17. Comparison of measured and estimated bending moments for NJM01 Event 11.

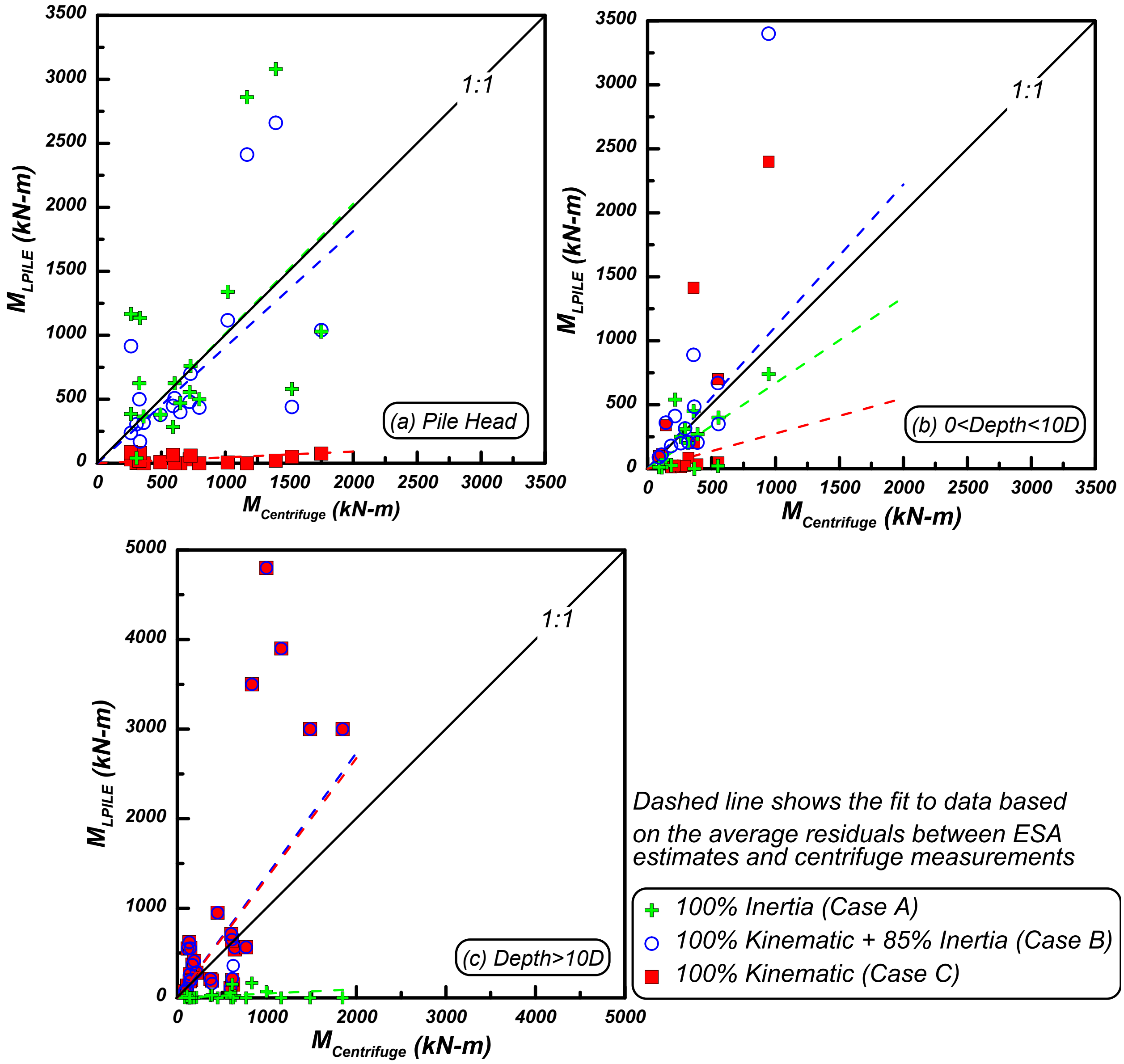

Fig. 18. Peak bending moments measured in centrifuge tests and estimated from ESA analyses in *LPILE* at (a) the pile head, (b) locations shallower than 10D, and (c) locations deeper than 10D.